Empirical formulation for multiple groups of primary biological ice nucleating particles from field observations over Amazonia

Sachin Patade, Vaughan T J Phillips, Pierre Amato, Heinz G Bingemer, Susannah M Burrows, Paul J Demott, Fabio L T Goncalves, Daniel A Knopf, Cindy E. Morris, Carl Alwmark, et al.

Empirical formulation for multiple groups of primary biological ice nucleating particles from field observations over Amazonia

Sachin Patade[1*], Vaughan T. J. Phillips[1], Pierre Amato[2], Heinz G. Bingemer[3], Susannah M. Burrows[4], Paul J. DeMott[5], Fabio L. T. Goncalves[6], Daniel A. Knopf[7], Cindy E. Morris[8], Carl Alwmark[9], Paulo Artaxo[10], Christopher Pöhlker[11], Jann Schrod[3], Bettina Weber[11,12]

[1]Department of Physical Geography and Ecosystem Science, Lund University, Lund, Sweden

[2]Université Clermont Auvergne, CNRS, SIGMA Clermont, ICCF, F-63000, Clermont-Ferrand, France

[3]Institute for Atmospheric and Environmental Science, Goethe University of Frankfurt, Frankfurt am Main, Germany

[4]Atmospheric Sciences and Global Change Division, Pacific Northwest National Laboratory, Richland, WA, 99354

[5]Department of Atmospheric Science, Colorado State University, Fort Collins, Colorado, USA

[6]Departamento de Ciências Atmosféricas, Instituto de Astronomia, Geofísica e Ciências Atmosféricas, Universidade de São Paulo, São Paulo, Brazil

[7]Institute for Terrestrial and Planetary Atmospheres, School of Marine and Atmospheric Sciences, Stony Brook University, Stony Brook, New York 11794-5000, USA

[8]INRAE, Pathologie Végétale, 84140, Montfavet, France

[9]Department of Geology, Lund University, Lund, Sweden

[10]Instituto de Física, Universidade de São Paulo, Brazil

[11]Multiphase Chemistry Department, Max Planck Institute for Chemistry, 55128 Mainz, Germany

[12]Institute of Biology, University of Graz, Austria

*** Corresponding Author**

Dr. Sachin Patade, Lund University, Sweden

email: sachin.patade@nateko.lu.se

Abstract:

To resolve the various types of biological ice nuclei (IN) with atmospheric models, an extension of the empirical parameterization (EP) (Phillips et al. 2008; 2013) is proposed to predict the active ice nuclei from multiple groups of primary biological aerosol particles (PBAPs). Our approach is to utilize coincident observations of PBAP sizes, concentrations, biological composition, and ice-nucleating ability. The parameterization organizes the PBAPs into five basic groups: fungal spores, bacteria, pollen, viral particles, plant/animal detritus, algae, and their respective fragments. This new biological component of the EP was constructed by comparing predicted and observed concentrations of PBAP IN at the Amazon Tall Tower Observatory (ATTO) site located in the central Amazon. In addition to the observations from the ATTO site, PBAP IN activity from the literature is used in constraining the fitting parameters of EP. The parameterization has empirically derived dependencies on the surface area of each group (except algae), and the effects of variability in their mean sizes and number concentrations are represented via their influences on the surface area. The concentration of active algal IN is estimated from literature-based measurements.

Predictions of this new biological component of the EP are consistent with previous laboratory and field observations not used in its construction. The EP scheme was implemented in a 0D parcel model. It confirms that biological IN account for most of the total IN activation at temperatures warmer than $-20^{\circ}\mathrm{C}$ and at colder temperatures dust and soot become increasingly more important to ice nucleation.

1 Introduction

Often referred to as bioaerosols, primary biological aerosol particles (PBAPs) are a subset of biogenic particles emitted from the Earth's surface. They consist of biological material such as viruses, algae, bacteria, fungal spores, pollen, plant and animal detritus, and their fragments and secretions. In the ambient atmosphere, bioaerosols may be present in the form of clusters, single particles, and agglomerates and exist in a variety of shapes such as rods, spirals, spherical, or spheroidal forms. A review article by Després et al. (2012) describes the typical concentrations of these PBAPs in the ambient air, their sizes, and sampling techniques. Bioaerosols can act as ice nuclei (IN) to initiate ice at temperatures often warmer than -12°C, well above the homogeneous freezing point (Prenni et al. 2009; DeMott and Prenni, 2010; Morris et al. 2012; Fröhlich-Nowoisky et al. 2016). To maintain consistency with previous EP papers (e.g. for mathematical symbols), we will use the term, 'IN' rather than 'ice nucleating particles' (INPs, Vali et al. 2015) for this paper. They can also act as giant cloud condensation nuclei (CCN) (Barahona et al. 2010; Delort et al. 2010) and may play an important role in the hydrological cycle. Bioaerosols may influence the formation of precipitation, especially in pristine air over densely vegetated areas (Phillips et al. 2009; Pöschl et al. 2010; Huffman et al. 2013; Prenni et al. 2013).

In warm-based convective clouds, rain production can occur through collision-coalescence that facilitates the heterogeneous raindrop freezing to form graupel ('*warm rain process'*). Heterogeneous nucleation of ice crystals and their subsequent growth to form snow and graupel particles ('*ice crystal process'*) plays an essential role in rain formation in convective clouds with higher clouds bases (e.g. Rogers and Yau, 1989; Pruppacher and Klett, 1997). The role of bioaerosols in altering cloud microphysical properties, precipitation, and ecosystem interactions has been recognized for many years and is a topic of increasing interest (e.g. Pöschl et al. 2010; Huffman et al. 2013; Amato et al. 2015). The PBAPs can play an

important role in altering the cloud microphysical processes and precipitation formation through warm rain processes. However, large uncertainty still exists regarding their potential to facilitate precipitation, particularly their impact on global or on regional scales (Hoose et al. 2010a; Morris et al. 2011).

As reviewed in Després et al. (2012), several previously published studies have reported ice nucleation activities of various biological species, including fungi, pollen, algae, and bacteria. Among various PBAP species, higher ice nucleation activity is observed for bacterial and fungal particles in clouds. The quantitative measurements of biological IN in the atmosphere are rare. Biological IN in the atmosphere exhibit strong temporal and spatial variations (Christner et al. 2008; Pouzet et al. 2017). For a better understanding of their impact on clouds, more quantitative measurements of biological IN in the Earth's atmosphere are required.

With the limited observations of biological IN, numerical models can serve as an important tool for investigating their effect on cloud microphysical processes and hence on precipitation. Using a 1.5-dimensional cloud model, Levin et al. (1987) studied the efficiency of cloud seeding with bacteria. Ariya et al. (2009) showed that biological IN could trigger cloud glaciation through ice multiplication processes. Diehl and Mitra (2015) implemented PBAPs (pollen and bacteria) in a parcel model using the ice-active mass site density approach (Kanji et al. 2017 and references therein) and found that they were not involved in significant ice formation. Hummel et al. (2018) implemented PBAPs in the regional atmospheric model. They showed that although PBAPs were very efficient IN at high subzero temperature, due to their low atmospheric concentration, it is difficult to quantify their impact on cloud properties. However, they also showed that PBAP can influence the cloud ice phase in the clouds with cloud temperatures below −15 ^{o}C in the absence of any other IN. Hiron and Flossmann (2015) studied the potential impact of the presence of bacteria as an extremely IN active PBAP on

cloud and rain development. They noticed a significant increase in the rainfall flux in the simulation with only bacteria as IN. However, in the simulations where all other IN modes were also forming ice, their influence on rainfall became negligible. Phillips et al. (2009) showed that an increase in PBAP resulted in more numerous cloud droplets through their CCN activity and reduced the precipitation production via warm rain process, boosting cloud lifetime and extent. In the case of higher bioaerosol, the extra heterogeneous ice from biological IN particles can only partially counteract that effect, indicating the CCN activity of PBAPs is more important than their IN activity for the simulated warm-based convection. Several studies have used regional as well as global models to understand the geographical variation and climatic importance of bioaerosols (e.g. Burrows et al. 2009a, b; Hoose et al. 2010a; Sesartic et al. 2012). The empirical data included in these models are highly uncertain. Most of the parameterizations of heterogeneous ice nucleation of biological particles are based on laboratory measurements or derived from theory.

Consequently, the cloud-resolving numerical models need to be constrained and confirmed by observational data of biological IN to have a better estimation of their effect on clouds. Using a 'bottom-up approach' (i.e. measurements of ice nucleation activity of biological species in the laboratory to represent atmospheric ice initiation) in the numerical models can introduce significant bias in the active IN concentrations because the particular biological species studied in the laboratory may not necessarily be a good representative of the corresponding wider PBAP population in the atmosphere. Instead, there is a need for a better parameterization of heterogeneous ice nucleation of biological IN that accounts for diversity in their physical and chemical characteristics in the atmosphere. We have followed a 'top-down' approach in the current study to resolve the ice nucleation activity of multiple groups of PBAPs collected directly from the atmosphere. The empirical parameterization (EP) for heterogeneous ice nucleation presented here is based on the active surface site density approach (e.g. Phillips

et al. 2008; Niemand et al. 2012; Kanji et al. 2017 and references therein). The assumption of active surface site density has some limitation on consistently describing freezing curves over a wide range of surface area as described in Beydoun et al. (2016). They suggested an alternative approach invoking a continuum assumption on the ice nucleating activity (contact angle) of an aerosol particle's surface which does not require any assumptions about the size or number of active sites.

The first empirical ice nucleation parameterization for biological particles was proposed by Phillips et al. (2008) where biological particles were assigned as a part of insoluble organic particles. An estimation of the number of active IN consisting of insoluble aerosol species assumed that it was approximately proportional to the total surface area of its aerosol particles. In the subsequent study, Phillips et al. (2013) revised the original EP scheme by replacing insoluble aerosol species by the new group specifically for PBAP IN. However, their scheme does not address the separate activity of various groups of PBAPs with different ice-nucleating abilities.

In the present study, a framework for parameterizing the heterogeneous ice nucleation of biological particles is formulated and accounts for contributions from various groups of PBAPs including

1) Fungal spores and associated fragments;
2) Bacteria and their fragments;
3) Pollen and their fragments;
4) Viral, plant/animal detritus;
5) Algae.

Matthias-Maser and Jaenicke (1995) first described these groups of PBAPs through observations. The EP's treatment applies to deposition and condensation-/immersion-freezing modes.

The proposed scheme is empirical, mostly based on coincident observations of PBAP size distributions and active biological IN sampled from the atmosphere over the Amazon Rainforest with abundant PBAPs. Prenni et al. (2009) have revealed that over the Amazon Rainforest the contribution of local biological particles to ice nucleation is increased at warmer atmospheric temperatures, whereas the contribution of dust particles is increased at colder temperatures, making this region ideal for biological IN measurements.

2 Material and methods

2.1 Measurement site

The samples for the present study were collected over the central Amazon basin at the Amazon Tall Tower Observatory (ATTO; Andreae et al. 2015). The ATTO site is in the middle of the Amazon Rainforest in northern Brazil (see Fig. 1), about 150 km northeast of Manaus (120 m above sea level) with coordinates S 2° 08' 45.13" W 59° 00' 20.12". The measurement facilities at the ATTO site consists of a 325 m tall tower and two 80 m towers, one of which is a triangular mast currently used for a wide set of aerosol measurements (Andreae et al. 2015). The immediate surroundings as well as the ATTO footprint region are covered by an old-growth undisturbed forest with minimal anthropogenic impact.

Meteorological conditions vary throughout the year with a wet (February–May), a dry (August-November), and a transition from wet to dry season (December-January) (Pöhlker et al. 2019). This classification of seasons is consistent with seasonality of atmospheric pollution, rainfall, and air mass origin. Over the Amazon rainforest the PBAPs are ubiquitous throughout the year (Martin et al., 2010). During the wet season, the atmospheric boundary layer over the Amazon is relatively clean with low aerosol number concentrations (Artaxo et al. 2002; Martin et al. 2010; Zhou et al. 2002) and the hydrological cycle is strongly influenced by biogenic aerosols. However, during the Amazonian dry season, the atmospheric aerosol concentrations are considerably higher due to biomass burning (Andreae et al., 1988; Artaxo et al., 2002; Pöhlker et al. 2018; Holanda et al. 2019) and mixed-pollution scenarios (Pöhlker et al. 2018). A detailed description of the aerosol size distribution and the CCN characteristics at the ATTO site are given by Pöhlker et al. (2016, 2018). Additional details on the diurnal temperature and wind variations, precipitation amount, and aerosol characteristics at the ATTO site can be found in Andrea et al. (2015).

Sampling was performed during the dry season in the Amazon between 5 and 18 September 2018. The sample collection was interrupted on a few days including September 9 and 15 due to damage to power supply, so sample collection was only possible for the twelve days mentioned in Figure 5a. As shown in Fig. 1, the sampling took place at the triangular mast site. The sampled air was carried through a stainless-steel tubing with a diameter of 0.75 inches to the aerosol sampling unit installed in a laboratory container located at the base of a triangular mast. A Total Suspended Particles (TSP) inlet was installed on a triangular mast at 60 m above ground level to ensure that the air was sampled above the canopy, which has an average height of ~23 meters. To avoid condensation in the filter holder, the sampled air from the TSP inlet was dried to a relative humidity < 40% using silica gel driers.

198 The inlet used for sample collection in the current study has been optimized to achieve
199 a maximum sampling efficiency (Moran-Zuloaga et al. 2018), however, a certain amount of
200 particle loss is unavoidable. The particles smaller than 100 nm are more prone to diffusive
201 losses and not relevant for the current study. Daniel Moran-Zuloaga et al. (2018) documented
202 potential losses in the accumulation and coarse mode particles of aerosol particles in this inlet
203 system which are more relevant to the current study. They calculated the transmission
204 efficiencies of the PBAPs for the inlet used in the current by using standard density of 1 g/cm^3
205 as best guess for typical PBAP densities. The aerosol transmission efficiency starts at about
206 100% (full transmission) for particles with diameter around 0.7 µm and then declines with
207 increasing particle size. Based on their calculation typical transmission efficiencies for PBAPs
208 with diameter 1, 2, 4, 8, and 10 µm were 98, 97, 91, 72, and 55% respectively. Correction to
209 PBAP size distributions was applied accordingly.

210 A detailed analysis about the back trajectories arriving at the ATTO site is presented
211 in Moran-Zuloaga et al. (2018) and Pöhlker et al. (2019). They showed that the ATTO-relevant
212 back trajectories followed a seasonal swing between a Northeast path during the wet season
213 and a Southeast path during the dry season as a response to the annual north–south Intertropical
214 Convergence Zone migration. Figure 1 shows the seven-day analysis from the Hybrid Single-
215 Particle Lagrangian Integrated Trajectory Model (Draxler and Rolph, 2003) on three sampling
216 days (11-13 September 2018) at 60 m above ground. Back trajectories revealed that the
217 anthropogenic emissions from Manaus did not significantly impact the sampled air mass,
218 however, the atmospheric conditions at the ATTO site during our sampling period were not
219 pristine.

220

221 **2.2 Aerosol measurements and sample collection**

222 *2.2.1 Aerosol size distribution measurements*

223 The aerosol size distribution and number concentration at the ATTO site was measured
224 by a Scanning Mobility Particle Sizer (SMPS; TSI Inc) and an Aerodynamic Particle Sizer
225 (APS; TSI Inc). The SMPS measures the electrical mobility diameter (10-430 nm), while the
226 APS gives aerodynamic diameters (0.5-20 µm) of the particles. There were frequent
227 interruptions in the aerosol measurements during our observational period due to severe
228 lightning strikes and associated damage to the power supply and installation. Therefore,
229 measurements of the aerosol size distribution from SMPS and APS was available only for a
230 few days.

231 *2.2.2 Aerosol collection by filter method*

232 Table 1 describes the sampling type, duration, flow rate, purpose, and corresponding
233 instrument in which the samples were analyzed. The aerosol samples were collected from
234 September 5-18, 2018, for a twelve-day period at the ATTO site. The collection of aerosol
235 samples for the drop freezing tests and microscopic analysis was carried out via the TSP inlet
236 through a four-stage stacked filter unit. Four Polytetrafluoroethylene (PTFE) membrane filter
237 papers (25 mm diameter) (Sartorius Stedim Biotech) with the pore sizes of 5 (outermost), 1.2,
238 0.45, and 0.2 (innermost) µm were used for the sampling. The filters were placed in an airtight
239 aluminum filter holder in order of decreasing pore size. Samples were collected with a vacuum
240 pump (VWR vacuum gas PM20405-86). The flow rate was controlled using a flow meter
241 (Kytola instruments) equipped with a needle valve. Collection efficiencies of PTFE membrane
242 filters of pore size 5 and 1.2 µm are much higher compared to Millipore and glass filters of
243 similar pore sizes (Soo et al., 2016) and thus inevitably most of the aerosol particles are
244 collected on the first two filters.

Cascade filter samples were collected with an average volumetric sample flow rate of 4 Lpm (Liters per minute) for approximately 4 hours each day. In addition, a set of cascade filters with a sample flow rate of 1.5 Lpm was collected for about 16 hours. A set of aerosol samples with a sample volume of about 200 L was collected using only a 0.2 μm filter to estimate IN concentrations activated by the immersion-freezing mode in Frankfurt Ice Nuclei Deposition Experiment (FRIDGE-IMM) chamber.

Samples were sealed carefully in a sterile container and stored at 4°C at the ATTO site. The aerosol samples when stored for prolonged time under such conditions, can show changes in their ice nucleation activity. Stopelli et al. (2014) found a degradation in the active IN concentration by a factor of two at temperature between −8 to −12°C in snow water samples stored at 4°C for 30 days. After the campaign was completed, the samples were transported to the University of Sao Paulo and later to Lund (Sweden). The samples were stored in a deep freezer at −25°C at Lund until they were analyzed by scanning electron microscopy **(**SEM) and drop freezing tests.

2.2.3 Aerosol collection by Programmable Electrostatic Aerosol collector (PEAC7)

In addition to the filter method, aerosol sampling was performed using a Programmable Electrostatic Aerosol collector (PEAC7) (Schrod et al. 2016). The PEAC samples were analyzed to estimate IN activated by deposition and condensation-freezing mode in the FRIDGE-STD chamber. A total of twelve samples were collected using PEAC during the field campaign held from September 5-18, 2018 (see Figure 5).

In addition, PEAC samples were used for imaging PBAPs under SEM. On each sampling day, aerosol particles were collected at a volumetric flow rate of 2 Lpm using the PEAC7 for 50 minutes. The PEAC7 unit used in the current analysis is based on the single wafer electrostatic aerosol collector described in Klein et al. (2010). In PEAC7, aerosol

particles are introduced through a central inlet into the field of electrons emitted by 12 gold electrodes. The aerosols are negatively charged and carried to the positively charged silicon (Si) wafers (Wacker-Siltronic, thickness: 0.7 mm, diameter: 45 mm) where they are deposited on the surface (Klein et al. 2010).

We have applied the correction to the IN concentrations and size distribution of bioaerosol particles by assuming the PEAC7 collection efficiency of 60% observed by Schrod et al. (2016). Klein et al. (2010) and Schrod et al. (2016) provide additional details on the design and working principle of PEAC7.

2.3 Scanning electron microscopy analysis

Primary bioaerosol particles were analyzed by using a variable pressure Tescan Mira3 High-Resolution Schottky FE-SEM located in the Geology department at Lund University. It should be noted that the SEM analysis was limited to three days: 9 (night-time; hereafter 0911N), 12 (day-time; hereafter 0912D) and 13 (day-time; hereafter 0913D) September, as an intensive collection of SEM images characterizing the size distributions for all the samples was not practical. During each of the three days, the size distribution and IN number were estimated for total biological aerosols (5 + 1.2 µm filters) and fractions obtained on 5 and 1.2 µm filters. Thus, nine pairs of measurements of active IN and size distributions were available from three intensive sampling days mentioned above and will be referred to as the nine ‘cases’ in the remaining part of the manuscript.

To reduce charging under the electron beam, the samples were coated with a thin layer (10 nm) of Palladium, sputter-deposited prior to the SEM analysis. The coated samples were examined at a beam size of 15 keV with a working distance of 10 mm. The working distance

was lowered (between 5 and 10 mm) for Si wafer samples to obtain clearer images of particles with diameter (D) < 1.5 µm.

To quantify the PBAPs, the main method of identification was purely based on the morphological characteristics, following the method of Matthias-Maser and Jaenicke (1991, 1994). The organic nature of particles from energy-dispersive X-ray spectrometer (EDS) analysis was confirmed if (C+O) > 75% and 1% < P, K, Cl < 10% (Coz et al. 2010). The SEM system used in the current study was equipped with an energy-dispersive X-ray spectrometer (EDS, X-Max^N 80, Oxford instruments, 124 eV, 80 mm^2). The EDS could detect the composition of individual particles semi-quantitatively for elements with an atomic number greater than 6 including light elements such as C, N, O. Errors in measurements of the composition of light elements by EDS vary for individual samples and are below 2 percent overall. The EDS was performed at a beam intensity of 15 keV with a working distance of 10 mm. The Si and F peaks in the EDS spectra were not considered for particles from the Si wafer and PTFE filter respectively, because of the interference from the substrate. The duration of each EDS collection was limited to 10-12 seconds to avoid particle damage. Because other elements like S, Ca, or Si can also be tracers of PBAPs, this analysis should be treated as a conservative estimate.

Before imaging the individual biological particles, wide reference areas each 100 x 100 µm in size were chosen randomly and corresponding images of those areas were saved as reference pictures along with their positions on the filter paper. Particles located in these predefined reference spots were counted, and high-resolution images were acquired for those particles. About five particles were observed roughly at each predefined reference spots on the filter samples. The maximum dimension of particles was recorded and saved. In this study the maximum dimension is treated as the diameter of the particle.

316 Based on the number of PBAPs detected in the scanned filter area, the bioaerosol
317 number was upscaled to the whole filter area. The size distribution of the PBAPs was classified
318 into 40 predefined size bins covering a size range from 0.2-40 µm. The measured number was
319 converted to an airborne concentration (per m^3 of air) based on the sampled air volume. The
320 recorded data was then used to classify the particles into the basic PBAP groups: fungal spores,
321 bacteria, pollen, viral particles, plant/animal detritus, algae, and their respective fragments. The
322 primary classification of PBAPs into different groups was based on similarity in morphological
323 characteristics with those reported in earlier studies. Despite all possible efforts to categorize
324 the identified PBAPs, not all of them could be attributed to any PBAP group. A small fraction
325 of the PBAPs (~ 5%) which did not find any similarity in morphology with the PBAP groups
326 considered here were classified as 'unidentified' PBAPs. These unidentified particles were not
327 included in the size distributions of PBAPs presented here.

328 Since the emphasis of the current study was to characterize the size distribution of
329 PBAPs, non-biological particles were excluded from the study. In addition to filter samples, Si
330 wafers were analyzed under SEM using similar methodology. Additional details about SEM
331 analysis including scanned area and number of bioaerosol images collected are given in Table
332 2. More than 0.1% of the total filter area was investigated under SEM and > 200 images were
333 collected for each sampling day considered for SEM analysis. For Si wafers, more than 0.06%
334 of the total area was scanned under SEM and ~100 images of PBAPs were collected.

335 Identification and counting of particles with $D < 1.5$ µm (e.g. bacteria) on filter samples
336 was challenging as they were often hidden inside the dense membrane of filter material.
337 Therefore, the size distribution of biological particles with $D < 1.5$ µm were determined mostly
338 by SEM imaging of Si wafers. This was justified as the size distributions from the Si wafer and
339 corresponding filter were in good agreement within the overlapping region between 1.5 and 5
340 µm. The collection efficiency of the 5 µm filter for various particle diameters was estimated

based on total aerosol number concentrations from the SMPS, APS and the size distribution of total particles collected on the 1.2 µm filter. The SMPS and APS aerosol size distributions used here were from 0914, a typical sampling day at the ATTO site. Based on the collection efficiency of the 5 µm filter, the size distributions of biological particles on 5 and 1.2 µm filters were estimated separately. The estimated collection efficiency for particles with a diameter between 0.3-6 µm was variable between 0.81 and 0.99 whereas it was unity for other size ranges. The collection efficiency of 1.2 µm filters was not measured and assumed to be unity (for particles with $D > 0.1$ µm) based on measurements by Soo et al. (2016).

After acquiring the images of bioaerosols from SEM analysis, we classified them into common PBAP groups based on size and morphology.

2.4 Flow cytometry analysis

In addition to SEM, we conducted flow cytometry (FCM) analysis to estimate the total bioaerosol number concentration. FCM is widely used to detect and measure the physical and chemical characteristics of cells or particles. This is a fluorescent technique, in which cells are often labeled with fluorescent markers so that light is absorbed and then emitted in a wavelength band. For each sample extract, cell counts were performed on 450 µL triplicates added with 50 µL 5% glutaraldehyde (stored at 4°C). For analysis, samples extracts were stained with SYBRGreen I (Molecular Probes Inc.). This stains nucleic acids, and thus reveals all DNA-containing particulate matter (e.g. viruses, bacteria, archaea, fungi, pollen, plant and animal cells). The parameters used with FCM did not detect chlorophyll, proteins, and carotenoids. The wavelengths for excitation and emission were 488 and 530 nm, respectively. The FCM counts were performed for 3 minutes. The flow cytometry technique used in the current analysis can detect particles as small as 0.3 µm (Lippé, 2018).

2.5 Measurement of Ice nucleating particles

IN in the air were measured using the FRIDGE chamber of Goethe University, Frankfurt. FRIDGE operates in two different modes: a) as a low pressure diffusion chamber (here called FRIDGE-STD) for the detection of deposition/condensation freezing IN collected onto Si wafers (see 2.2.3), and b) as a cold stage freezing array (here called FRIDGE-IMM) for the measurement of immersion freezing IN in extracts of filter samples (see 2.2.2). Additional details have been described in previous studies (Klein et al., 2010; Schrod et al., 2016; DeMott et al., 2018, 2018a).

2.5.1 Measurement of IN activated by deposition and condensation freeing mode using FRIDGE-STD

The FRIDGE-STD method applies a static low-pressure diffusion chamber for activation, growth and counting of IN activated at temperatures between 0 and -30°C. For analysis, a Si wafer substrate that was previously laden with electrostatically precipitated aerosol particles (using PEAC-7) was placed on the cold stage in the chamber. The chamber was then closed, evacuated, and cooled to the desired temperature. The surface temperature was measured using a PT-1000 sensor. In the next step, water vapour was introduced into the chamber by opening the connection to the vapour source. The supersaturation with respect to ice over the Si wafer was then estimated as the ratio of vapour pressure in the chamber over saturation vapour pressure at the surface temperature. The number of activated ice crystals grown was counted using automatic picture analysis software. All the twelve samples collected on Si wafer by PEAC-7 were processed for IN activation in the FRIDGE-STD mode (see Figures 5a-c).

2.5.2 Measurement of IN activated by immersion freezing mode using FRIDGE-IMM:

389 The number concentrations of IN in the air activated by immersion freezing mode were
390 measured on the cold stage of FRIDGE-IMM with the drop freezing method of Vali (1971), as
391 described by Ardon-Dryer and Levin (2014) and DeMott et al. (2018). The aerosol samples
392 collected on 0.2 μm filters were used for the drop freezing experiment. Each filter was placed
393 in 5 ml of deionized water and stirred vigorously for a few minutes to create particle
394 suspensions. Around 60 droplets, each with a volume of 2.5 μL were pipetted onto on a clean,
395 salinized Si wafer, with the chamber almost closed, but at ambient atmospheric pressure. The
396 temperature of the cold stage was lowered by 1°C min^{-1}. A steady flow of synthetic air of 1 L
397 min^{-1} through the chamber to avoid the condensation and rime effects. The number of drops
398 that froze as function of temperature was recorded by the charge-coupled device (CCD)
399 camera. Two runs of drop freezing experiments were conducted for each sample. In FRIDGE-
400 IMM, eleven filter samples were treated to measure the IN concentrations activated by
401 immersion freezing mode (see Figure 5d).

402 *2.5.3 Quantification of biological IN*

403 The concentration of biological IN in the air, active between $-5^{\circ}C$ and $-15^{\circ}C$, was
404 determined by conducting the drop freezing experiments in the LED-based Ice Nucleation
405 Detection Apparatus (LINDA) LINDA chamber as described below. The detailed technical
406 information and working principle of LINDA are described by Stopelli et al. (2014) and
407 summarized here. The LINDA device has an array (7 × 8) of red LEDs (Light Emitting Diodes;
408 645 nm wavelength). This array is mounted on a printed circuit board casted into a
409 polycarbonate housing and submersed in a cold bath. A liquid sample is distributed in a total
410 of 52 sample tubes (0.5 mL Eppendorf). These tubes are held in another polycarbonate plate
411 and placed onto the LED array so that each tube is located above one LED. The temperature is
412 recorded by four sample tubes with cast-in Pt-1000 temperature sensors placed in the corner
413 positions of the tube holder.

Before starting the freezing experiment, 75% of each filter sample was placed in 30 mL of deionized water to create suspensions, of which 20 ml was used for the freezing experiment in LINDA. The remaining 25% of the filter was saved and stored in a petri dish for SEM analysis. The filter samples were cut using sterilized scalpel. To make the LINDA sample extract clearer to facilitate the imaging, 2 ml of NaCl (in liquid form, 0.8% w/v) was added to the solution. Adding NaCl to the LINDA sample extracts should not affect its freezing characteristics since no freezing event was noticed for the solution containing deionized water and NaCl. The remaining 10 ml solution was saved and stored in a refrigerator (at 4°C) for subsequent flow cytometry.

The sample extract is distributed in a total of 52 sample tubes each of which contain 400 µL of the sample extract. The samples were analyzed at the cooling rate of 0.4°C min^{-1}. Images of the tubes are recorded every six seconds using a Monochrome camera, during which temperature was changed by 0.04°C. For each filter sample extract, two sets of freezing experiments were carried out. In the first set of experiments, sample extracts were untreated (no heating) for total IN concentration measurements. In the second set, the samples were heated to 95°C for 10 minutes to denature the IN activity of biological IN following Christner et al. (2008) and Garcia et al. (2012). The concentrations of active biological IN were calculated as the difference between the concentrations of active IN measured with and without heating. However, it should be noted that heat treatment may not inactivate every ice nuclei site of biological material and hence the values presented should be considered as the lowest possible estimates of biological IN.

Previous findings based on heat treatment (e.g. Garcia et al. 2012; Joly et al. 2014) showed that the relative contribution of biological IN decreases with temperature, with 97% to 100% of total IN active at −8°C and 77% at −12°C as other particles including dust, become active at colder temperatures. Hill et al. (2014) showed that heat treatment (at 95°C) of bacterial

samples obtained by leaf washing reduced the ice nucleation activity by >75% at −10°C. According to Conen et al. (2011), heating to 100°C reduced IN active at −12°C by 70–98%. O'Sullivan et al. (2015) showed that heat treatment (90°C) of soil samples containing organic decomposing matter reduced ice nucleation activity at −12°C to ~1/10.

In addition, the concentration of active biological IN at temperatures colder than −15 °C was estimated for the sample extract of 0911 (from section 2.5.1) based on heating tests (95°C for 10 minutes) in FRIDGE-IMM. The methodology of drop freezing experiment is already described in section 2.5.1.

2.6 Classification of PBAPs based on SEM images

After collecting the bioaerosol images, we classified them into common PBAP groups based on size and morphology. Table 3 presents the general size and morphological characteristics of different PBAP groups, based on the literature available. These characteristics form the basis for classifying PBAPs SEM images into basic groups. Typical images of the bioaerosols collected from each group during this study are shown in Fig. 2.

Fungal spores and associated fragments (group 1) were one of the most common classes of bioaerosols observed during the campaign. Fungi can grow in almost every ecosystem and are efficient in aerosolization (Adhikari et al., 2009; Löbs et al. 2020). The morphological characteristics of fungal spores have been well documented in global air and are summarized in Table 3 (Després et al. 2012 and references therein; Shi et al. 2003; Tamer Vestlund et al. 2014; Valsan et al. 2015; Valsan et al. 2016; Priyamvada et al. 2017; Wu et al. 2019, Li et al. 2020). They appear in various forms including globular, sub-globular, elliptical, and elongated. Many of the spores possess the attachment scar and appear either with smooth or ornamented surfaces. The size range of particles from SEM images considered for classification of PBAPs

in this group is generally from 1 to 20 μm. The SEM images of fungal spores collected over Amazon rainforest (e.g. Huffman et al. 2012, Cybelli et al. 2018, China et al. 2016) were also referred while conducting the classification.

The images of bacteria (group 2) on Si wafer were clearer and were used for the size distribution. The basic morphological features of bacterial particles are spheres (coccus) and round-ended cylinders (bacillus). In addition, there may be few others with helically twisted shapes. Some bacterial cells grow separately while some rods or cocci grow in chains, grapelike clusters or form a cubic packet characteristically. The surface structures include flagella, pili, and capsules. A few representative images of bacillus and cocci shaped bacteria from the ATTO samples are shown in Fig. 2. We attempted to grow the bacteria from filter samples in agar solution, but no bacterial growth was observed. It should be noted that the filter samples were not immediately analyzed for bacterial growth and were stored in a freezer at $-25^{\circ}C$ after sampling, which could have affected the number of viable bacteria.

The pollen grains (group 3) were broadly distinguished from fungal spores based on size and morphology. Typically, its size ranges from 10 to 100 μm. PBAPs are classified into pollen based on the general morphological characteristics of pollen grains given in table 3. Cybelli et al. (2018) provided an extensive image database of pollen grains collected at the ATTO site and was frequently used for classification. From our SEM imaging, the size range of the pollen grains varied between 8 and 20 μm. The pollen grains with a diameter of 10 to 30 μm were frequently observed at the ATTO site and the large pollen grains were absent high above the canopy except during some thunderstorm events (Cybelli et al. 2018). Accordingly, our SEM analysis did not show pollen grain presence greater than 20 μm. Observed pollen grains exhibited different shapes including ellipsoid, fusiform, globose/spheroidal.

For a given scanned area under SEM, 2-4 brochosome clusters have been detected on the filter for each case and are assigned to group 4. (viral, plant/animal detritus). Each cluster consists of 3 to 40 brochosomes with an individual diameter of about 0.45 µm. Brochosomes are intricately structured microscopic granules secreted by leafhoppers that are typically found on their body surface and more rarely, eggs (Wittmaack, 2005). The group 4 was dominated by the presence of leaf litter followed by epicuticular wax of plants, insect scales, and other vegetation detritus. The viral particles were hardly accessible in our SEM analysis.

Somewhat surprisingly, during a rather large number of SEM investigations, no particle could be identified as algae (group 5; Sect. 1) and therefore algae are not shown in the size distribution presented here. A near-by water source close to the ATTO site had no measurable impact on algal aerosol number concentration. However, algae can grow on leaves and soil. They could also be part of the long-range transport of marine particles from the Atlantic Ocean into the Amazon Rainforest (Martin et al. 2010; Moran-Zuloaga et al. 2018). Backward trajectories (at 2 km) using the HYSPLIT model (see Fig. 1) suggest that a marine air mass from the Atlantic Ocean would have travelled over 5-6 days to reach the ATTO site. In summary, the absence of algae in our SEM analysis can be attributed to their low concentration in the air at the ATTO site and possible limitation in identifying them using SEM.

The identification and classification of fragments of various PBAP is challenging due their complex and irregular shape. Consideration was given to the external features of the background PBAPs on the filter paper that were easy to detach from main PBAP particle. On this basis, the fragments in the form of external spines, hyphae, etc. are then assigned to the parent particle. In addition, the characteristics of the cell wall and other visible features of the fragments have been closely examined to identify its parent PBAP with matching features. The

fragments smaller than 1 μm that were not in the form of distinguished external features of main particle are difficult to classify and referred to here as unidentified particles.

3 Results and discussion

3.1 The size distributions of PBAPs based on SEM analysis:

Based on the SEM analysis of the filter and Si wafer samples, the size distributions for total bioaerosol as well as for various PBAP groups were constructed for 0911N, 0912D, and 0913D and are shown in Fig. 3. In general, no difference in the size distribution of total PBAPs between day and nighttime samples is observed. The 'coarse mode' (diameter 1-10 μm) bioaerosol particles were dominated by fungal spores as the corresponding size distribution shows a peak between 3-4 μm. This is in agreement with the previous measurements by Huffman et al. (2012) and Whitehead et al. (2016), in which they attributed the peak in the coarse fluorescent biological size distribution to fungal spores. Several types of fungal spores such as *Basidiomycota, Cladosporium, Inocybe calospora, Rhizopus* were frequently observed. Most pollen grains observed during SEM were with $D > 8$ μm. 'Fine mode' ($D < 1$ μm) bioaerosol particles were dominated by the plant or animal detritus as well as bacteria. Overall, the total size distribution of PBAPs from the current study is in good agreement with previous observations by Huffman et al. (2012) and Whitehead et al. (2016) from a similar geographical location (see Figure 3d).

The mean number concentrations of four PBAP groups including fungi, bacteria, pollen, and viral, plant/animal detritus from SEM analysis are given in Table 3. Typically the

number concentrations of fungal spores and pollens at the ATTO are ~10^4 m^{-3} and ~10^3 m^{-3} respectively, following typical concentrations in vegetated areas (Després et al. 2012 and references therein). The estimated mean number concentrations of bacterial particles is ~10^5 m^{-3}, which is greater by one order of magnitude than their typical concentration of ~10^4 m^{-3} in the air (Després et al. 2012 and references there-in).

To get an idea regarding the size distribution of total aerosol particles during the campaign, a combined aerosol size distribution from the SMPS and APS on 0914 is shown in Fig. 3d. The SMPS and APS data were not available at the ATTO site for other sampling days considered here, as these instruments were not working on those days. Using aerosol size distributions (by SMSP+APS) on 0914 as a reference, ~11% of coarse mode aerosol particles are of biological origin.

The total PBAP number concentration (with D > 0.3 μm) from SEM was compared with their independent estimations with FCM as shown in Fig. 4. Overall, a good agreement is observed between SEM and FCM estimation of total PBAP number concentration for samples from all three days discussed here. The number concentration of PBAPs from FCM was slightly lower than those from SEM, since abundance of PBAPs by FCM represents an approximately lower limit for the actual abundance of PBAPs. The concentrations of fluorescent biological aerosol particles (FBAP) from the FCM analysis were 3.3×10^5, 1.06×10^6, and 1.19×10^6 m^{-3} for 0911N, 0912D, and 0913D respectively. These values are consistent with previously reported FBAP concentrations of about $2 \times 10^5 - 1.2 \times 10^6$ m^{-3} by Whitehead et al. (2016) in the central Amazon forest. Huffman et al. (2012) reported coarse mode FBAP concentration of about 7.3×10^4 m^{-3} over Amazon rainforest.

3.2 Observations of total IN

The observations of total IN including deposition and condensation-freezing IN and immersion freezing IN are shown in Fig. 5. Figure 5 (a, b, and c) shows the concentration of IN activated by deposition and condensation-freezing modes determined as a function of temperature and relative humidity over ice (RH_{ice}) obtained by the FRIDGE-STD measurements. No active IN at temperatures warmer than −20°C were detected with this instrument, suggesting that their concentrations may have been lower than the detection threshold of 0.01 L^{-1}. For a given temperature and RH_{ice}, a large day-to-day variability in IN concentration was observed. The results indicate that higher IN concentration was associated with higher RH_{ice} at a given temperature. The mean IN concentration at −25°C ranged from 0.03 to 0.43 L^{-1} for RH_{ice} between 120% and 130%. During the field campaign, the highest concentration of deposition and condensation freezing IN measured by FRIDGE-STD was 4.5 L^{-1} at −30°C.

Figure 5d shows the cumulative number concentration of immersion freezing IN from separate experiments in LINDA and FRIDGE-IMM as a function of temperature. Overall, the concentration of immersion freezing IN was in the range of 0.0027-40 L^{-1} at temperature between −6 to −30°C. Absence of any active IN in FRIDGE-IMM at temperature > −15°C could be associated with IN concentrations below the detection threshold of 0.15 L^{-1}. The sample volume for LINDA samples was higher than the FRIDGE-IMM samples (see Table 1), as a result LINDA had a lower detection threshold of 0.0014 L^{-1}. The concentrations of IN from FRIDGE-STD at water saturation are lower than the concentrations of immersion freezing IN from FRIDGE-IMM as FRIDGE-STD does not encapsulate the full immersion freezing.

3.3 Biological IN concentration from drop freezing experiments

The cumulative concentrations of biological and non-biological IN determined by drop freezing arrays in LINDA are represented in Fig. 6 for 0911N, 0912D, 0913D. The concentration of active biological IN between -5°C and -15°C was determined by comparing measurements with and without heating. Freezing was observed with wide variance in onset temperature. Heating the sample extracts decreased the highest temperature of freezing, by 1°C in 0911N and 0913D to more than 4°C in 0912D. The active biological IN concentrations in air ranged from 0.0015 to 0.047 L^{-1} between -6.5°C and -15°C and are in the range of previous biological IN measurements from rain samples (e.g. Bowers et al. 2009; Xia et al. 2013; Pouzet et al. 2017). In general, the relative contribution of biological IN to the total IN decreased with decreasing temperature. The relative contribution of biological particles in the sample extracts of 0911N and 0912D ranged from ~100% of the total IN active at -8°C to as low as ~ 86% at -15°C. In comparison, the contribution of biological particles to the total IN concentration in the sample extract of 0913D was much lower (~ 62% at -13°C).

4. Empirical parametrization of heterogeneous ice nucleation for multiple groups of biological particles

4.1 General equations for prediction of biological IN number concentration

4.1.1 Overview of existing empirical parametrization of heterogeneous ice nucleation

The EP of deposition and condensation-/immersion-freezing modes was proposed originally by Phillips et al. (2008, 2013). They assumed that for any scenario of aerosol loading, the number mixing ratio of active IN has contributions from the three groups including

dust/metallic, black carbon, and organic aerosols. Thus, the number mixing ratio of active IN can be written as

$$n_{IN} = \sum_{X} n_{IN,X} \qquad (1)$$

where X = DM, BC, BIO and solO for dust/metallic, black carbon, primary biological and soluble organic aerosols, respectively.

The number concentration of active IN activated by deposition and condensation-/immersion-freezing modes from group X is proportional with aerosol surface area as:

$$n_{IN,X} = \int_{\log[0.1\ \mu m]}^{\infty} \{1 - \exp[-\mu_X]\} \times \frac{dn_X}{d\log D_X} d\log D_X, \qquad (2)$$

$$\mu_X = H_X(S_i, T)\ \xi(T) \left(\frac{\alpha_X n_{IN,1,*}}{\Omega_{X,1,*}}\right) \times \frac{d\Omega_X}{dn_X} \quad \text{for } T < 0\ ^{\circ}\text{C and } 1 < S_i < S_i^w \qquad (3)$$

The Ω_X is the total surface area of all aerosols with dry diameters larger than 0.1 μm, μ_X is the average of the number of activated ice embryos per insoluble aerosol particle of size D_X. The number mixing ratio of aerosols in group X is given by n_X. A simplified version of Eqs (2) and (3) are used for X=solO. The term $H_X(S_i, T)$ is the empirically determined fraction ($0 \leq H_X \leq 1$) representing scarcity of nucleation under substantially subsaturated conditions. The α_X is a fractional contribution from aerosol group X to the IN concentration.

The number of ice crystals generated in a time step Δt is given by

$$\Delta n_i = \sum_X \left(n_{IN,X} - n_{X,a}, 0\right) \equiv \sum_X \Delta n_{X,a} \qquad (4)$$

where $n_{X,a}$ is the number mixing ratio of IN from group X that has already been activated. Additional details about the scheme and associated terms can be found in Phillips et al. (2008; 2013)

4.1.2 Modification in the existing scheme for parametrization of biological IN based on PBAP IN examined here and literature

The original EP treated biological ice nucleation with only one species of IN. That assumption is changed as follows.

Here we now replace the previous *X*= BIO by five PBAP groups (1)-(5) (Sec. 1) including fungal spores and associated fragments (FNG), pollen and their fragments (PLN), bacteria and their fragments (BCT), viral, plant/animal detritus (DTS), and algae (ALG). According to the EP for atmospheric ice nucleation by Phillips et al. (2008), the concentration of active IN from the given group within the given size interval $d\log D_X$ depends on surface areas of given aerosol species. The empirical formulation mentioned below was not applied to algal particles since their size distribution from SEM measurements was not available. We used literature values of their frozen fraction to measure their ice nuclei activity, and will be discussed in the later part of this section.

For *X*= FNG, PLN, BCT, and DTS

$$n_{IN\_BIO,X} = \int_{\log\,[0.1\ \mu m]}^{\infty} \{1 - \exp\,[-\mu_X]\} \times \frac{dn_X}{d\log D_X} d\log D_X, \qquad (5)$$

$$\mu_X = H_X(S_i, T)\ \xi(T)\ \times \mathrm{MIN}\{[\exp(-\gamma_X T) - 1], 40\}\ \times \frac{1}{\omega_{X,1*}} \frac{d\Omega_X}{dn_X} \quad \text{for } T < 0\ ^{\circ}\mathrm{C} \qquad (6)$$

Here, $n_{IN\_BIO,X}$ is the number mixing ratio of IN active at temperature *T* in the X^{th} bioaerosol species; Ω_X is the total surface area mixing ratio of particles with diameters D_X greater than 0.1 µm in group *X* and is a prognostic variable of the atmospheric model; $d\Omega_X/dn_X \approx \pi D_X^2$; $dn_X/d\log D_X$ is the normalized size distribution of given bioaerosol species *X*. The absence of smaller particles with diameter 0.1-0.2 µm that were not measured during SEM analysis is associated with technical limitation of setup. This is expected to have an insignificant effect

on our empirical formulation as the contribution of these smaller particles to the overall surface area mixing ratio is negligible. In the empirical formulation provided here, the surface area of a particle is more important than its mass. For 0911N, the contribution of particles in the size bin 0.1-0.2 μm to the total surface area mixing ratio is about 0.15% when the number concentration of particles in this size bin was assumed to be similar to that of in the neighboring size bin with larger diameter. Shape factors should also be considered when estimating the surface area of PBAPs. However, due to the complexity of the observed shapes of PBAPs we assumed spherical shape for all PBAPs and refrained from considering the shape factor in the estimation of surface area.

The factor μ_X is the average number of potentially activated ice embryos per aerosol particle with diameter D_X. For lower freezing fractions $\mu_X \ll 1$, the Eq (6) can be written as $n_{IN\_BIO,X} = H_X(S_i,T)\,\xi(T)[\exp(-\gamma_X T) - 1] \times \Omega_X/\omega_{X,1*}$ showing surface area dependence of predicted IN number concentrations. The $\omega_{X,1*}$ is an unknown parameter and depends on bioaerosol type with the dimensions of area (m^2). In Eq (6), $H_X(S_i,T)$ is the empirically determined fraction ($0 \le H_X \le 1$) representing suppression of nucleation under substantially water-subsaturated conditions. The H_X is expressed as a function of S_i and T by Phillips et al. (2008) with H_X =1 at water saturation. The slope of the fitted curve predicting activated IN is given by γ_X. The factor ξ considers the fact that drops are not observed to freeze at temperatures warmer than a threshold in the laboratory observations. Phillips et al. (2008) proposed $\xi = \delta_1^0\,(T, T_1, T_2)$, where ξ is 1 for $T < T_1$ and 0 for $T > T_2$ with cubic interpolation between and assumed T_1 (-5°C) and T_2 (-2°C) for all aerosol species.

For temperatures colder than -20°C, lower slope values (45% of original) of the fit were prescribed based on observations of biological IN of 0911N at temperature between

668 -20°C and -27°C (see Fig. 9). The modified version of proposed parameterization (eq. 6 and

669 7) for any $T < 0^{\circ}$C can be written as

670 $$n_{IN\_BIO,X} = \int_{\log[0.1\ \mu m]}^{\infty} \{1 - \exp[-\mu_X]\} \times \frac{dn_X}{d\log D_X} d\log D_X, \qquad (7)$$

671 $$\mu_X = \begin{cases} H_X(S_i, T)\ \xi(T)\ \times \mathrm{MIN}\{[\exp(-\gamma_X T) - 1], 40\} \times \frac{1}{\omega_{X,1*}} \frac{d\Omega_X}{dn_X}, & \text{for } T > -20°\mathrm{C} \\ H_X(S_i, T)\ \xi(T) \times \mathrm{MIN}\{[\exp(-\gamma_X T) - 1], 40\} \times \exp[0.45 \times (T + 20)] \times \frac{1}{\omega_{X,1*}} \frac{d\Omega_X}{dn_X} \\ , \text{otherwise} \end{cases}$$

672 (8)

673 Eqs (7) and (8) are applied for biological species, X = FNG, PLN, BCT, and DTS (groups 1-

674 4, Sec. 1)

675 Regarding algal particles (group 5; Sec. 1), a separate representation is proposed as

676 follows. Since the concentrations of algal particles at the ATTO site were much lower than

677 our detection threshold (~ 0.5 m^{-3}) we could not use a similar empirical treatment for them as

678 was used for other PBAP groups. Generally, in atmospheric models there may be situations

679 where algae are more prolific and can influence the ice initiation. In such a scenario, their

680 contribution to the total biological IN can not be excluded. We therefore used the estimation

681 of the frozen fraction for the algal particles (Diatom cell, *T. pseudonana*) available in the

682 literature (Wilson et al. 2015) to estimate the algal IN in the atmosphere. The relationship

683 between the frozen fraction (f_{algae}) of algae and temperature was established and (see

684 extended data Fig. 6 in Wilson et al. 2015) is given by

685 $$f_{algae}(T) = A_1 + \frac{(A_2 - A_1)}{1 + 10^{(B+T)\times p}} \qquad (9)$$

686 here $A_1 = -0.03, A_2 = 0.993, B = 27.73,$ and $p = 0.399$.

687 with $f_{algae}(T) = 0$ at $T > -24\ ^{o}C$ and $f_{algae}(T) = 1$ at $T < -35\ ^{o}C$

If the concentration of algal particles (n_{algae}) in the air is known, then for *X*= ALG

$$n_{IN\_BIO,X} = f_{algae} \times n_{algae} \quad (10)$$

Our scheme treats the algal particles over the ocean but does not apply to the prediction of biogenic organic macromolecules which can act as efficient IN. Although they are biological in origin, these organic macromolecules are not classified as PBAPs as they are dissolved organic matter and therefore not primary (Knopf et al. 2018; Pummer et al. 2012; Pummer et al. 2015; McCluskey et al. 2018). These ice nucleating macromolecules are accessible on the surfaces of leaves, wood and bark and can be washed down by rainwater (Felgitsch et al. 2018).

4.2 Empirical determination of values of parameters

Based on the IN (Fig. 7 and C1) and size distribution measurements (see Fig. 3 and B1) for nine cases mentioned earlier, the values of active biological IN from groups (1)-(4) were estimated using proposed EP (Eqs. 5-8). Experiment-based estimate of all unknown parameters for each PBAP category is constrained by several technical aspects of PBAP collection and processing for ice nucleation. A key problem we faced in the observation of our samples was size distribution of various PBAP groups overlap greatly. Consequently, it was not possible to isolate each PBAP group on a single filter. In addition, two of the four PBAP groups, including pollen and leaf litter, naturally have lower IN activity compared to fungi and bacteria (Després et et al. 2012 and references therein). We have tried to overcome these difficulties by collecting our samples on different days under contrasting conditions in conjunction with inverse modeling. But there was a limit to the number of parameters that could be constrained by the inverse modelling. Some of these parameters were therefore constrained based on laboratory measurements available in the literature.

711 The values of slope parameter γ at $T > -15^{\circ}$C are prescribed based on observations
712 made by Vali (1994, equation 8 therein) and are assumed to be similar among PBAP groups
713 (1)-(4) (Sec. 1). This assumption has the basis as the slope of the observed biological IN
714 concentration is consistent with the observations of Pouzet et al. (2017) (See Figure 7). The
715 concentration of total active biological IN from the EP is then compared to the observed
716 biological IN concentrations for each of the nine cases (see Fig 7 and C1). The relative
717 abundance of the four groups of PBAPs and IN concentrations varies between the nine
718 contrasting cases. For agreement between observed and parameterized values, the least-square
719 fitting was used to estimate the universal law applicable to all nine cases to resolve the
720 optimized values of the unknown parameters for PBAP groups (1)-(4).

721 The optimum values of the parameters inferred for the empirical scheme are shown in
722 Table 4. It should be noted that in the variational analysis the values of unknown parameter
723 $\omega_{X,1*}$ of comparatively less active PBAP groups including pollen and viral, plant/animal
724 detritus were constrained so that their estimated IN activity match the laboratory observation
725 reported in the literature. The estimations of $\omega_{X,1*}$ for group (4) are based on previous
726 observations of leaf litter (major part of group 4) from the tropics by Schnell and Tan-Schnell
727 (1982). For pollen, the $\omega_{X,1*}$was constrained based on laboratory observations on active sites
728 per gram of pollen mass (*Betula pendula*) by O'Sullivan et al. (2015). Additional details about
729 these measurements used in the construction of the EP are given in Table 5.

730 In the current study, the values of T_1 and T_2 for determining the factor ξ are assumed to
731 be variable for each bioaerosol type and are estimated based on the literature of previous
732 observations or laboratory measurements. Therefore, the values of T_1 and T_2 for each PBAP
733 group are denoted by $T_{X,1}$ and $T_{X,2}$. Several studies have documented the activation of pollen at
734 temperatures colder than -10°C (Després et al. 2012; Kanji et al. 2017, and references therein).
735 Freezing tests on leaf litter showed its activation at temperatures ~ -7°C (Schnell and Tan-

736 Schnell, 1982; Després et al. 2012). Based on these observations, T_1 was assumed to be −10 to
737 −7°C for pollen and plant/animal detritus respectively. Comparatively, fungi and bacteria are
738 activated at temperatures warmer than −5°C (Richard et al. 1996; Després et al. 2012; Kunert
739 et al. 2019) and therefore −7°C and −2°C, respectively, were assumed for T_1 of both.

740 Fig. 7 and C1 shows the predicted number concentrations of crystals nucleated by
741 various biological species based on size distributions from the total and 5, 1.2 µm filters,
742 respectively. The predicted values of total biological IN by the EP are of similar magnitude in
743 comparison with observations from the total (5 + 2 µm) and 5 µm filters. The total number
744 concentration was dominated by fungi and bacteria. The contributions from pollen and detritus
745 were lower by two orders of magnitude than those from fungi and bacteria at a given
746 temperature. Pollen grains can swell and explode from high humidity exposure to emit
747 numerous nanoscale particles which are 10 to thousand times smaller than intact particles.
748 These smaller fragments may become aerosolized and act as efficient IN (O'Sullivan et al.
749 2015; Knopf et al. 2018). Given this, the contributions of pollen grains to total biological IN
750 may be more important than suggested by our measurements. The predicted total IN
751 concentration is lower by 1-2 order magnitude when compared with the values obtained for the
752 1.2 µm filters (See Fig. C1). It can be attributed to the uncertainties in estimating the collection
753 efficiency of 5 µm filters and hence to the size distributions of bioaerosol particles on 1.2 µm
754 filters.

755

756

757 ## 5 Comparison of the empirical scheme with independent observations

758 The new EP is also compared with previous laboratory data and field observations, not
759 used in its construction, as shown in Figure 7 and C1. Additional details on the origin of these

760 data sets and corresponding calculations are given in Table 5. The total concentration of PBAP
761 IN predicted by EP is in good agreement with previous observations for rainwater samples
762 from Opme (France) by Pouzet et al. et al. (2017). For fungi, estimations of nucleation sites per
763 gram of fungal mass (*Fusarium avenaceum*) (O'Sullivan et al. 2015) and active IN per fungus
764 *(Basidiomycota spores)* (Haga et al. 2014) were used to calculate their contribution as IN for
765 the observed mass and number concentration of fungi over the Amazon. According to previous
766 studies by Murray et al. (2012) and references there-in., the number concentration of birch
767 pollen as potential IN is 2×10^{-3} m^{-3} at $-15^{\circ}C$. Based on ice nucleation activity of bacteria
768 isolated from cloud water by Joly et al. 2014, number concentrations of potential INA bacteria
769 were estimated ~ 0.32 and 5.8 m^{-3} of cloud air at temperatures −6 and $-8^{\circ}C$ respectively.
770 Murray et al. (2012) estimated the concentration of pollen IN at $-15^{\circ}C$ is 2.4×10^{-3} m^{-3}. The
771 active IN concentration from leaf litter per m^3 of air based on measurements by Schnell and
772 Vali (1976) for leaf litter from tropical regions is also shown for comparison with
773 parameterized values. When the uncertainty limits are considered, the EP's predicted PBAP IN
774 concentrations are in agreements with available literature data.

775 To represent ice nucleation abilities of various PBAP groups various metrics are used
776 in the previous studies. Most used metric includes 1) ice-active surface site densities (n_s), 2)
777 ice-active mass site densities (n_m), an analogue to n_s, but mass equivalent, 3) activated fraction
778 (Kanji et al. 2017 and references therein). To represent proposed EP in terms of these common
779 metric, we estimated the mean values of n_s, n_m for various PBAP groups based on PABP IN
780 activity, their surface area mixing ratio, and mass in nine cases considered in the study. Figure
781 8 shows the dependence of these variable from the EP on temperature. The values of these two
782 parameters for limited species of PBAP groups from the available literature are also shown for
783 reference. However, there is a considerable spread in the literature data.

784 At a given temperature, our estimated values of n_s and n_m for PLN and DTS by EP
785 were much lower (by three orders of magnitude) when compared with our prediction of FNG
786 and BCT as observed in the literature data (Kanji et al. 2017 and references therein). The values
787 of n_m for group 4 (mostly leaf litter) are in good agreement with literature data. The literature
788 values of n_s and n_m for snowmax and *Pseudomonas syringae* bacteria are much higher than
789 our estimated values (see Figure 8). For a given PBAP group, the published observations of n_s
790 and n_m show large variations among different biological species (Kanji et al. 2017 and
791 references therein) which limits their direct comparison with our estimated values of the EP,
792 which apply to entire groups of PBAPs. At a temperature of −10°C, for example, n_m of three
793 species of fungal spores showed variation over four orders of magnitude.

794

795

796 # 6 Application of empirical parameterization in a parcel model for an
797 # idealized case

798 The EP is applied in an idealized 0D parcel model to shed light on some ramifications
799 for natural ice initiation arising from the formulation. It should be noted that there are no
800 microphysical processes included inside the parcel model except for the heterogeneous ice
801 nucleation. The adiabatic parcel starts at 20°C, rises to −50°C and humidity is prescribed
802 corresponding to exact water saturation. Input size distributions of PBAPs (group 1-4) to the
803 empirical scheme are prescribed based on observations from the case 0911N. An EP from
804 Phillips et al. (2013) was applied for IN species including dust, soot and PBAPs. The
805 climatological values (from Model of Ozone and Related Chemical Tracers [*MOZART]*) of
806 mass mixing ratios for dust (2.9×10^{-10} kg/kg) and soot (3×10^{-11} kg/kg) over the ATTO
807 site were prescribed for estimating their contribution as IN. The total PBAP size distributions

were prescribed based on observations on 0911N. For algae, quantitative measurements of their abundance in the ambient air are rare. The algal particles were not included in the parcel model simulation shown here.

Figure 9 shows the predicted number concentration of active biological IN from multiple species as well as the total IN. Compared with Phillips et al. (2013), the total biological IN predicted by the proposed empirical scheme differs by maximum one orders of magnitude at $T > -15^{\circ}$C and by half order of magnitude at $T < -15$ ^{o}C. It should be noted that the EP by Phillips et al. (2013) does not resolve individual groups of PBAPs and was based on the ice nucleation of a bacterial strain observed in the laboratory that may not represent the large variations in ice nucleation characteristics observed among different PBAP groups. Overall, total IN concentrations predicted by the model are in good agreement with the concentrations observed at the ATTO site. The relative contributions to the total IN concentration of the different PBAP groups as well as dust and soot particles from this simulation are shown in Figure 10. Biological particles dominate the predicted total IN concentrations at a temperature warmer than -20°C and at colder levels dust and soot particles became increasingly important in determining the total IN concentrations in the cloud.

7 Conclusions

A modification to the flexible framework for treating multiple species of atmospheric IN in terms of empirical observations from the real atmosphere, namely the 'empirical parameterization' is proposed in the current study. The previous single species for biological IN has been replaced by five major PBAP groups including FNG, PLN, BCT, DTS, and ALG. The new treatment has been fitted to the coincident observations of ice nucleation activity of

PBAPs and their size distributions based on observation from a field campaign at the ATTO site located in the central Amazon. In addition to the observations of PBAP IN from the ATTO site, the literature data are used for the construction of the EP. The new empirical treatment will allow atmospheric models to explicitly resolve the IN activity of these PBAP groups.

PBAPs were collected on PTFE membrane filters and Si wafers for use in drop freezing experiments, ice nuclei activation in cloud chamber, and SEM/EDX analysis. An EP was constructed to predict the active IN from multiple groups of PBAPs based on coincident observations of PBAP size, concentration, and ice-nucleating ability.

The measured IN concentrations activated by deposition and condensation-freezing modes varied over three orders of magnitude throughout the campaign and strongly depended on the processing temperature and ice supersaturation in the chamber. At -25^{o}C, the measured IN concentrations activated by deposition and condensation-freezing mode ranged from 0.002 L^{-1} to 1 L^{-1} for ice supersaturations of 21% and 28% respectively. The filter samples were analyzed in LINDA to estimate biological IN active between -5 and -15^{o}C. Filter and Si wafer samples were analyzed under SEM to measure the size distribution of common PBAP species. For each case, more than 300 images of bioaerosol particles were used for this purpose.

The observed bioaerosols included brochosomes, fungal spores, bacteria, canopy debris (e.g. leaf and insect fragments, plant waxes), and less commonly pollen and insect scales. Overall, size distributions were observed to be bimodal and were like previous measurements from similar geographical locations (e.g. Huffman et al. 2012; Whitehead et al. 2016). The observed size distributions of PBAP groups have provided constraints primarily on their surface areas in determining their ice nucleation activity. The size distribution of total bioaerosol particles was consistently dominated by a submicron peak associated with the viral, plant and animal detritus and bacteria. The coarse mode of PBAP observed in the current study was dominated by fungal spores consistent with previous observations (e.g. Huffman et al.

2012). The total number concentration of bioaerosols (with $D > 0.3$ μm) inferred by our SEM analysis is in good agreement with FCM analysis.

The total number concentration of biological IN predicted by the proposed parameterization scheme was dominated by fungi and bacteria followed by pollen and detritus. For PBAP groups considered in the construction of the scheme, the values predicted from the scheme and independent observational data not used in the construction of the scheme were consistent with concentrations of the same order of magnitude. Implementation of the scheme in the 0D parcel model showed that the biological IN account for most of the total ice nuclei activation at temperatures $> -20^{\circ}$C. At colder temperatures dust and soot become increasingly more important to ice nucleation. Previous observations in the Amazon basin by Prenni et al. (2009) also emphasize the importance of biological IN in determining total IN concentrations at warmer atmospheric temperatures. They showed that the dust became increasingly more important for ice nucleation at temperatures colder than -27^{o}C. In their transmission electron microscopy, no soot IN was observed, suggesting that biomass-burning particles were not a likely source of the carbonaceous IN. However, it should be noted that their observations were limited to the wet season. The biomass burning conditions are characteristics of the Amazon dry season and are maximum around September. Thus, the soot particles resulting from the biomass burning can play an important role in determining the ice nucleation at colder temperature during the dry season, as suggested by our parcel model simulation. It should be noted that the relative contributions of dust and soot to the ice nucleation shown in our parcel mode simulations are limited to a case study and it will be highly variable depending on their abundance in the atmosphere.

Data Availability Statement

The data that support the findings of this study are available from the corresponding author, Sachin Patade, on reasonable request. A copy of the EP scheme including the present addition is also available on request.

Acknowledgments

The work was funded by an award to Phillips (VTJP) from the Swedish Research Council ('Vetenskapsradet'), related to investigation of bio-aerosol effects on clouds (award number: 2015-05104). VTJP directed the study. For the operation of the ATTO site, we acknowledge the support by the Max Planck Society, the German Federal Ministry of Education and Research (BMBF contracts 01LB1001A, 01LK1602A and 01LK1602B) and the Brazilian Ministério da Ciência, Tecnologia e Inovação (MCTI/FINEP contract 01.11.01248.00) as well as the Amazon State University (UEA), FAPEAM, LBA/INPA and SDS/CEUC/RDS-Uatumã. This paper contains results of research conducted under the Technical/Scientific Cooperation Agreement between the National Institute for Amazonian Research, the State University of Amazonas, and the Max-Planck-Gesellschaft e.V.; the opinions expressed are the entire responsibility of the authors and not of the participating institutions. Further, we would like to thank all people involved in the technical, logistical, and scientific support of the ATTO project. All aerosol samples collected at the ATTO site are property of the University of São Paulo. Paul DeMott acknowledges support from the U.S. Department of Energy, Office of Science (BER), Atmospheric System Research (DE-SC0018929) and U.S. National Science Foundation Award #1660486. Daniel Knopf acknowledges support by the U.S. Department of Energy, Office of Science (BER), Atmospheric System Research (DE-SC0016370 and DE-SC0020006) and NASA award

NNX17AJ12G. Heinz G. Bingemer and Jann Schrod acknowledge funding by Deutsche Forschungsgemeinschaft (DFG) under the Research Unit FOR 1525 (INUIT) and from the European Union's Seventh Framework Programme (FP7/2007-2013) project BACCHUS under grant agreement no. 603445. Susannah Burrows acknowledges support by the U.S. Department of Energy (BER), through the Early Career Research Program. The authors gratefully acknowledge the NOAA Air Resources Laboratory (ARL) for the provision of the HYSPLIT transport and dispersion model. SP and VJTP would like to thank Dr. Thara Prabhakaran for providing the filter holder. We are very grateful to Marcin Jackowicz Korczynski and Tomas Karlsson for providing the vacuum pump and other sampling tools. The authors wish to thank Tina Šantl-Temkiv, Sylvie Tesson, Jakob Löndahl, and Cybelli Barbosa for their help with SEM image analysis and valuable suggestions. We are grateful to Reiner Ditz, Andrew Crozier, and Stefan Wolff for their help with organizing logistics for the visit to the ATTO site.

APPENDIX A

List of symbols

"Table A1 here"

APPENDIX B

PBAP Size distribution from 5 and 1.2 μm filter

"Figure B1 here"

APPENDIX C

Model prediction of biological particles for 5 and 1.2 μm filters

"Figure C1 here"

APPENDIX D

Implementation of empirical parameterization in an atmospheric model

The present EP scheme slots into the EP framework for heterogeneous ice nucleation already described in Phillips et al (2008, 2013). Their framework represents all modes of heterogeneous ice nucleation. The EP described in this study is for ice nucleation through deposition, condensation- and immersion-freezing mode.

To implement the scheme in a cloud model, each group X of IN is partitioned into prognostic components which are interstitial and immersed in cloud droplets to reflect the in-cloud scavenging of IN by precipitation. Extra scalars were introduced to track the depletion

in the number mixing ratio of interstitial IN by becoming immersed in cloud liquid without necessarily freezing ($n_{X,a,liq}$) and the actual number mixing ratio of immersed IN ($n_{X,\mathrm{imm}}$). The cut off size for immersed and interstitial IN size distributions is determined by ($n_{X,a,liq}$) and mixing ratio of aerosol in group X (Q_X). To include the heterogeneous freezing of raindrops a temporary grid of size bins was created to discretize their size distribution. If the mass mixing ratio of each bin is dQ_r, the number of IN particles in the rain that activate in time Δt is given by

$$d(\Delta n_{IN,rain}) \approx \Delta t \mathrm{MIN}[(w - v_t)\frac{\partial T}{\partial z}, 0]\ \frac{d}{dT}[\exp(-\gamma_X T) - 1] \sum_X \frac{d\Omega_{X,rain}}{\omega_{X,1,*}} \quad (11)$$

For a given raindrop size bin $d\Omega_{X,rain} = \Omega_{X,rain}\frac{dQ_r}{Q_r}$ is the surface area mixing ratio of IN within the raindrops. The fall velocity of raindrops is given by v_t, while w is the vertical air velocity.

We have adopted the approach followed by Phillips et al. (2008) for inside-out contact freezing. It assumes that a given IN has a freezing temperature for the contact nucleation which is $\Delta T_{CIN} \approx 4.5^{\circ}\mathrm{C}$ higher than for the immersion and condensation freezing mode. The number mixing ratio of potentially active, interstitial IN activated by contact freezing ($n_{X,cn}$) is given by

$$n_{X,cn} \cong \xi(T)\ \{\exp[-\gamma_X(T - \Delta T_{CIN})] - 1\} \sum_X \frac{d\Omega_{X,int}}{\omega_{X,1,*}} \quad (12)$$

Here, $\Omega_{X,int}$ is the component of Ω_X for interstitial IN.

971 **References:**

972 Adhikari, A., J. Jung, T. Reponen, J. S. Lewis, E. C. DeGrasse, and co-authors, 2009:
973 Aerosolization of fungi, (1-->3)-beta-D Glucan, and Endotoxin from materials collected
974 in New Orleans homes after hurricanes Katrina and Rita. General Meeting of the
975 American Society of Microbiology. *Environ. Res*., 109, 215-224.

976 Amato, P., M. Joly, C. Schaupp, E. Attard, O. Möhler, C. E. Morris, Y. Brunet, and A. M,
977 Delort, 2015: Survival and ice nucleation activity of bacteria as aerosols in a cloud
978 simulation chamber. *Atmos. Chem. Phys*., 15, 6455–6465, doi.org/10.5194/acp-15-6455-
979 2015.

980 Andreae, M. O., E. V. Browell, M. Garstang, G. L. Gregory, R. C. Harriss, G. F. Hill, D. J.
981 Jacob, M. C. Pereira, G. W. Sachse, A. W. Setzer, P. L. S. Dias, R. W. Talbot, A. L.
982 Torres, and S. C. Wofsy, 1988: Biomass-burning emissions and associated haze layers
983 over Amazonia, *J. Geophys. Res*., 93, 1509–1527,
984 https://doi.org/10.1029/JD093iD02p01509.

985 Andreae, M. O., O. C. Acevedo and Coauthors, 2015: The Amazon Tall Tower Observatory
986 (ATTO): Overview of pilot measurements on ecosystem ecology, meteorology, trace
987 gases, and aerosols. *Atmos. Chem. Phys.*, **15**, 10 723–10 776,
988 doi:https://doi.org/10.5194/acp-15-10723-2015.

989 Ardon-Dryer, K. and Z. Levin, 2014: Ground-based measurements of immersion freezing in
990 the eastern Mediterranean, *Atmos. Chem. Phys*., 14, 5217–5231.

991 Ariya P. A., J. Sun, N. A. Eltouny, E. D. Hudson, C. T. Hayes & G. Kos, 2009: Physical and
992 chemical characterization of bioaerosols–Implications for nucleation
993 processes. *International Reviews in Physical Chemistry*, 28:1, 1-
994 32, DOI: 10.1080/01442350802597438.

995 Artaxo, P., J. V. Martins, M. A. Yamasoe, A. S. Procópio, T. M. Pauliquevis, M. O. Andreae,
996 P. Guyon, L. V. Gatti, and A. M. Cordova Leal, 2002: Physical and chemical properties
997 of aerosols in the wet and dry seasons in Rondônia, Amazonia. *J. Geophys. Res*., 107,
998 8081, https://doi.org/10.1029/2001JD000666.

999 Barahona, D., R. E. L. West, P. Stier, S. Romakkaniemi, H. Kokkola, and A. Nenes, A., 2010:
1000 Comprehensively accounting for the effect of giant CCN in cloud activation
1001 parameterizations. *Atmos. Chem. Phys*., 10, 2467–2473, doi:10.5194/acp-10-2467-2010.

1002 Beydoun, H., M. Polen, and R. C. Sullivan, 2016: Effect of particle surface area on ice active
1003 site densities retrieved from droplet freezing spectra, Atmos. Chem. Phys., 16, 13359–
1004 13378, https://doi.org/10.5194/acp-16-13359-2016.

1005 Burrows, S. M., W. Elbert, M. G. Lawrence, U. and Pöschl, 2009a: Bacteria in the global
1006 atmosphere – Part 1: Review and synthesis of literature data for different ecosystems.
1007 *Atmos. Chem. Phys*., 9, 9263–9280, doi:10.5194/acp-9-9263-2009.

1008 China S., B. Wang, J. Weis, L. Rizzo, J. Brito, G. G. Cirino, L. Kovarik, P. Artaxo, M. K.
1009 Gilles, and A. Laskin, 2016: Rupturing of biological spores as a source of secondary
1010 particles in Amazonia. *Environ. Sci. Technol.* **50**, 12179–12186 (2016)

1011 Christner B. C., R. Cai, C. E. Morris, K. S. McCarter, C. M. Foreman, M. L. Skidmore, S. N.
1012 Montross and D. C. Sand , 2008: Geographic, seasonal, and precipitation chemistry
1013 influence on the abundance and activity of biological ice nucleators in rain and snow. *P.*
1014 *Natl. Acad. Sci*., 18854-18859.

1015 Conen, F., C. E. Morris, J. Leifeld, M. V. Yakutin, and C. Alewell, 2011: Biological residues
1016 define the ice nucleation properties of soil dust. *Atmos. Chem. Phys*., 11, 9643–9648,
1017 https://doi.org/10.5194/acp-11-9643-2011

1018 Cybelli Barbosa, 2018: Primary biological aerosol particles at the Amazon tall tower
1019 observatory: inventory and vertical distribution, Ph.D. dissertation.

1020 Delort A.M., M.Vaïtilingom P. Amato, M.Sancelme, M. Parazols, G. Mailhot, P. Laj, L.A
1021 Deguillaume, 2010: short overview of the microbial population in clouds: potential roles
1022 in atmospheric chemistry and nucleation processes. *Atmos. Res*., 98, pp. 249-260.

1023 DeMott P. J., A. J. Prenni, 2010: New Directions: Need for defining the numbers and sources
1024 of biological aerosols acting as ice nuclei, *Atmospheric Research*, 15, 1944-1945.

1025 DeMott, P. J., O. Möhler, , D. J. Cziczo, N. Hiranuma, M. D. Petters, S. S. Petters, F. Belosi,
1026 H. G. Bingemer, , S. D. Brooks, C. Budke, M. Burkert-Kohn, K. N., Collier, A.
1027 Danielczok, O. Eppers, L. Felgitsch, S. Garimella, H. Grothe, , P. Herenz, T. C. J. Hill,
1028 K. Höhler, Z. A. Kanji, A. Kiselev, T. Koop, T. B. Kristensen, K. Krüger, G. Kulkarni,
1029 E. J. T. Levin, B. J. Murray, A. Nicosia, D. O'Sullivan, A. Peckhaus, M. J. Polen, H. C.
1030 Price, N. Reicher, D. A. Rothenberg, Y. Rudich, G. Santachiara, T. Schiebel, J. Schrod,
1031 T. M. Seifried, F. Stratmann, R. C. Sullivan, K. J. Suski, M. Szakáll, H. P. Taylor, R.
1032 Ullrich, J. Vergara-Temprado, R. Wagner, T. F. Whale, D. Weber, A. Welti, T. W.
1033 Wilson, M. J. Wolf, and J. Zenker, 2018: The Fifth International Workshop on Ice
1034 Nucleation phase 2 (FIN-02): laboratory intercomparison of ice nucleation
1035 measurements, *Atmos. Meas. Tech*., 11, 6231–6257.

1036 DeMott, P. J., O. Möhler, , D. J. Cziczo, N. Hiranuma, M. D. Petters, S. S. Petters, F. Belosi,
1037 H. G. Bingemer, , S. D. Brooks, C. Budke, M. Burkert-Kohn, K. N., Collier, A.
1038 Danielczok, O. Eppers, L. Felgitsch, S. Garimella, H. Grothe, , P. Herenz, T. C. J. Hill,
1039 K. Höhler, Z. A. Kanji, A. Kiselev, T. Koop, T. B. Kristensen, K. Krüger, G. Kulkarni,
1040 E. J. T. Levin, B. J. Murray, A. Nicosia, D. O'Sullivan, A. Peckhaus, M. J. Polen, H. C.
1041 Price, N. Reicher, D. A. Rothenberg, Y. Rudich, G. Santachiara, T. Schiebel, J. Schrod,

T. M. Seifried, F. Stratmann, R. C. Sullivan, K. J. Suski, M. Szakáll, H. P. Taylor, R. Ullrich, J. Vergara-Temprado, R. Wagner, T. F. Whale, D. Weber, A. Welti, T. W. Wilson, M. J. Wolf, and J. Zenker, 2018a: Supplement of The Fifth International Workshop on Ice Nucleation phase 2 (FIN-02): laboratory intercomparison of ice nucleation measurements, *Supplement of Atmos. Meas. Tech*., 11, 6231–6257, 2018

Després, V., J. A. Huffman, S. M. Burrows, C. Hoose, A. S. Safatov, G. Buryak, J. Fröhlich-Nowoisky, W. Elbert, M. O. Andreae, U. Pöschl, and R. Jaenicke, 2012: Primary biological aerosol particles in the atmosphere: A review, *Tellus B Chem. Phys. Meteorol.* 64 (1):15598. doi:10.3402/tellusb.v64i0.15598.

Diehl K., S. Matthias-Maser, R. Jaenicke, S.K Mitra, 2002: The ice nucleating ability of pollen: Part II. Laboratory studies in immersion and contact freezing modes, *Atmospheric Research*, Volume 61, Issue 2, Pages 125-133,

Diehl, K. and S. K. Mitra, 2015: New particle-dependent parameterizations of heterogeneous freezing processes: sensitivity studies of convective clouds with an air parcel model, Atmos. Chem. Phys., 15, 12741–12763, https://doi.org/10.5194/acp-15-12741-2015.

Draxler, R. R. and G. D. Rolph, 2003: HYSPLIT (HYbrid Single-Particle Lagrangian Integrated Trajectory) Model access via NOAA ARL READY Website, http://ready.arl.noaa.gov/HYSPLIT.php, NOAA Air Resources Laboratory, Silver Spring, MD.

Felgitsch, L., P. Baloh, J. Burkart, M. Mayr, M. E. Momken, T. M. Seifried, P. Winkler, D. G. Schmale III, and H. Grothe, 2018: Birch leaves and branches as a source of ice-nucleating macromolecules, Atmos. Chem. Phys., 18, 16063–16079.

Fröhlich-Nowoisky, J., C. J. Kampf, B. Weber, J. A. Huffman, C. Pöhlker, M. O. Andreae, N. Lang-Yona, S. M. Burrows, S. S. Gunthe, W. Elbert, H. Su, P. Hoor, E. Thines, T.

1066 Hoffmann, V. R. Després, and U. Pöschl, 2016: Bioaerosols in the Earth system: Climate,
1067 health, and ecosystem interactions. *Atmos. Res.*, 182, 346–
1068 376, https://doi.org/10.1016/j.atmosres.2016.07.018.

1069 Fröhlich-Nowoisky, J., T. C. J. Hill, B. G. Pummer, G. D. Franc, and U. Pöschl, 2015: Ice
1070 nucleation activity in the widespread soil fungus Mortierella alpina. Biogeosciences, 12,
1071 1057–1071, doi:10.5194/bg-12-1057-2015.

1072 Garcia E., T. C. J. Hill, A. J. Prenni, P. J. DeMott, G. D. Franc, and S. M. Kreidenweis, 2012:
1073 Biogenic ice nuclei in boundary layer air over how U.S. high plains agriculture regions.
1074 *J. Geophy. Res*., 117, D018209.

1075 Govindarajan A. G., S. E. Lindow, 1988: Size of bacterial ice-nucleation sites measured in situ
1076 by radiation inactivation analysis, *PNAS*, 85(5):1334-1338. DOI:
1077 10.1073/pnas.85.5.1334.

1078 Haga, D. I., S. M. Burrows, R.Iannone, M. J. Wheeler, R. H. Mason, J. Chen, E. A. Polishchuk,
1079 , U.,Pöschl, and A. K.Bertram, 2014: Ice nucleation by fungal spores from the classes
1080 Agaricomycetes, Ustilaginomycetes, and Eurotiomycetes, and the effect on the
1081 atmospheric transport of these spores. *Atmos. Chem. Phys.*, 14, 8611–8630,
1082 doi:10.5194/acp-14-8611-2014.

1083 Hill T., Moffett B. F., Demott P. J., Georgakopoulos D. G., Stump W. L., Franc G. D.
1084 2014: Measurement of ice nucleation-active bacteria on plants and in precipitation by
1085 quantitative PCR. *Appl. Environ. Microbiol.* 80 1256–1267. 10.1128/AEM.02967-13.

1086 Hiron, T., A. I. Flossmann, 2015: A study of the role of the parameterization of heterogeneous
1087 ice nucleation for the modeling of microphysics and precipitation of a convective
1088 cloud. *J. Atmos. Sci.* **2015**, *72*, 3322–3339.

Holanda, B. A., Pöhlker, M. L., Saturno, J., Sörgel, and co-authors, 2019: Influx of African biomass burning aerosol during the Amazonian dry season through layered transatlantic transport of black carbon-rich smoke, *Atmos. Chem. Phys. Discuss*., https://doi.org/10.5194/acp-2019-775.

Hoose, C. and O. Möhler, 2012: Heterogeneous ice nucleation on atmospheric aerosols: a review of results from laboratory experiments, *Atmos. Chem. Phys*., 12, 9817–9854.

Hoose, C., J. E. Kristjansson, and S. M. Burrows, 2010a: How important is biological ice nucleation in clouds on a global scale*? Environ. Res. Lett*., 5, 024009, doi:10.1088/1748-9326/5/2/024009.

Huffman, J. A., A. J. Prenni, P. J. DeMott, C. Pöhlker, R. H. Mason, N. H. Robinson, J., Fröhlich-Nowoisky, Y. Tobo, V. R. Després, E. Garcia, D. J. Gochis, E. Harris, I. Müller-Germann, C. Ruzene, B. Schmer, B. Sinha, D. A. Day, M. O. Andreae, J. L. Jimenez, M. Gallagher, S. M. Kreidenweis, A. K. Bertram, and U. Pöschl, 2013: High concentrations of biological aerosol particles and ice nuclei during and after rain. *Atmos. Chem. Phys.*, 13, 6151–6164, https://doi.org/10.5194/acp-13-6151-2013.

Huffman, J. A., B. Sinha, R. M. Garland, A. Snee-Pollmann, S. S. Gunthe, P. Artaxo, S. T., Martin, M. O. Andreae, and U. Poschl, 2012: Size distributions and temporal variations of biological aerosol particles in the Amazon rainforest characterized by microscopy and real-time UV-APS fluorescence techniques during AMAZE-0. *Atmos. Chem. Phys*., 12, 11997–12019, doi:10.5194/acp-12-11997-2012.

Hummel, M., C. Hoose, B. Pummer, C. Schaupp, J. Fröhlich-Nowoisky, and O. Möhler, 2018: Simulating the influence of primary biological aerosol particles on clouds by heterogeneous ice nucleation, *Atmos. Chem. Phys*., 18, 15437–15450, https://doi.org/10.5194/acp-18-15437-2018.

1113 Joly, M., P. Amato, L. Deguillaume, M. Monier, C. Hoose, and A. M. Delort, 2014:
1114 Quantification of ice nuclei active at near 0 °C temperatures in low-altitude clouds at the
1115 Puy de Dôme atmospheric station. *Atmos. Chem. Phys*., 14, 8185–8195.

1116 Kanji, Z. A., L .A. Ladino, H. Wex, Y. Boose, M. Burkert-Kohn, D.J. Cziczo, and M.
1117 Krämer, 2017: Overview of Ice Nucleating Particles. *Meteorological*
1118 *Monographs*, 58, 1.1–1.33.

1119 Klein, H., W. Haunold, U. Bundke, B. Nillius, T. Wetter, S. Schallenberg, and H. Bingemer,
1120 2010: A new method for sampling of atmospheric ice nuclei with subsequent analysis in
1121 a static diffusion chamber. *Atmos. Res*., 96, 218–224,
1122 doi:10.1016/j.atmosres.2009.08.002.

1123 Knopf, D. A., P. A. Alpert, and B. Wang, 2018: The role of organic aerosol in atmospheric ice
1124 nucleation: A review. *ACS Earth and Space Chemistry*, **2**(3), 168– 202.

1125 Kunert, A. T., M. L. Pöhlker, K. Tang, C. S. Krevert, C. Wieder, K. R. Speth, L. E. Hanson,
1126 C. E. Morris, D. G. Schmale III, , U. Pöschl, J. Fröhlich-Nowoisky, 2019:
1127 Macromolecular fungal ice nuclei in Fusarium: effects of physical and chemical
1128 processing. *Biogeosciences*, 16, 4647-4659. doi: 10.5194/bg-16-4647-2019.

1129 Levin Z, S. A. Yankofsky, D. Pardes, N. Magal, 1987: Possible application of bacterial
1130 condensation freezing to artificial rainfall enhancement. *Biotechnol. Prog*. 26:1188–
1131 1197.

1132 Li W., L. Liu, L. Xu, J. Zhang, Q. Yuan, X. Ding, W. Hu, P. Fu, D. Zhang, 2020: Overview of
1133 primary biological aerosol particles from a Chinese boreal forest: Insight into
1134 morphology, size, and mixing state at microscopic scale. *Atmospheric Research*, Volume
1135 719, https://doi.org/10.1016/j.scitotenv.2020.137520.

Lippé R., 2018: Flow Virometry: A Powerful Tool To Functionally Characterize Viruses. *J Virol.* Jan 17;92(3). pii: e01765-17. doi: 10.1128/JVI.01765-17.

Löbs, N., C. G. G. Barbosa, S. Brill, D. Walter, F. Ditas, M. de Oliveira Sá, A. C. de Araújo, L. R. de Oliveira, R. H. M. Godoi, S. Wolff, M. Piepenbring, J. Kesselmeier, P. Artaxo, M. O. Andreae, U. Pöschl, C. Pöhlker, and B. Weber, 2020: Aerosol measurement methods to quantify spore emissions from fungi and cryptogamic covers in the Amazon. *Atmos. Meas. Tech*., 13, 153–164, https://doi.org/10.5194/amt-13-153-2020.

Martin, S. T., M.O. Andreae, P. Artaxo, D. Baumgardner, Q. Chen, A. H. Goldstein, A. Guenther, C. L. Heald, O. L. Mayol-Bracero, P. H. McMurry, T. Pauliquevis, U. Pöschl, K. A. Prather, G. C. Roberts, S. R. Saleska, M. A. S. Dias, D. V. Spracklen, E. Swietlicki, I. Trebs, I., 2010: Sources and properties of Amazonian aerosol particles. *Rev. Geophys*. 48.

Matthias-Maser S and R. Jaenicke, 1991: A method to identify biological aerosol particles with radius > 0.3 µm for the determinations of their size distribution. *J. Aerosol Sci*., 22:S849-S852.

Matthias-Maser, S., and R. Jaenicke, 1995: The size distribution of primary biological aerosol particles with radii .0.2 mmin an urban/rural influenced region. Atmos. Res., 39, 279–286.

Matthias-Maser, S., R. Jaenicke, 1994: Examination of atmospheric bioaerosol particles with radii greater than 0.2 mm. *J. Aerosol Sci*. 25, 1605e1613.

McCluskey, C. S., T. C. J. Hill, C. M. Sultana, O. Laskina, J. Trueblood, M. V. Santander, and co-authors, 2018: A mesocosm double feature: Insights into the chemical makeup of marine ice nucleating particles. *J. Atmos. Sci.*, 75(7), 2405–2423.

1159 Moran-Zuloaga, D., F. Ditas, D. Walter, J. Saturno, J. Brito, S. Carbone, X. Chi, I. Hrabe de
1160 Angelis, H. Baars, R. H. M. Godoi, B. Heese, B. A. Holanda, J. V. Lavric, S. T. Martin,
1161 J. Ming, M. L. Pöhlker, N. Ruckteschler, H. Su, Y. Wang, Q. Wang, Z. Wang, B. Weber,
1162 S. Wolff, P. Artaxo, U. Pöschl, M. O. Andreae, and C. Pöhlker, 2018: Long-term study
1163 on coarse mode aerosols in the Amazon rain forest with the frequent intrusion of Saharan
1164 dust plumes, *Atmos. Chem. Phys*., 18, 10055–10088, https://doi.org/10.5194/acp-18-
1165 10055-2018

1166 Morris C. E, D. C. Sands, M. Bardin, R. Jaenicke, B. Vogel, C. Leyronas, P. Ariya, R.
1167 Psenner, 2011: Microbiology and atmospheric processes: research challenges concerning
1168 the impact of airborne micro-organisms on the atmosphere and climate. *Biogeosciences*,
1169 8, 17-25, https://doi.org/10.5194/bg-8-17-2011.

1170 Morris, C. E., D. C. Sands, C. Glaux, J. Samsatly, S. Asaad, A. R. Moukahel, F. L. T.
1171 Goncalves, and E. K. Bigg, 2012: Urediospores of Puccinia spp. and other rusts are
1172 warm-temperature ice nucleators and harbor ice nucleation active bacteria. *Atmos. Chem.*
1173 *Phys. Discuss*., 12, 26143–26171, doi:10.5194/acpd-12- 26143-2012.

1174 Murray, B. J., D. O′Sullivan, J. D. Atkinson, M. E. Webb, 2012: Ice nucleation by particles
1175 immersed in supercooled cloud droplets. *Chem. Soc. Rev*. 41, 6519–6554.

1176 Niemand, M., O. Möhler, B. Vogel, H. Vogel, C. Hoose, P. Connolly, H. Klein, H. Bingemer,
1177 P. DeMott, J. Skrotzki, and T. Leisner, 2012: A Particle-Surface-Area-Based
1178 Parameterization of Immersion Freezing on Desert Dust Particles. *J. Atmos.*
1179 *Sci.,* 69, 3077–3092, https://doi.org/10.1175/JAS-D-11-0249.1

1180 O′Sullivan, D., B. Murray, J. F. Ross, T. F. Whale, H. C. Price, J. D. Atkinson, N. S, M. E.
1181 Webb, 2015: The relevance of nanoscale biological fragments for ice nucleation in
1182 clouds. *Sci Rep* 5, 8082, doi:10.1038/srep08082.

1183 Phillips V. T. J, P. J. DeMott, C. Andronache, 2008: An empirical parameterization of
1184 heterogeneous ice nucleation for multiple chemical species of aerosol. *J. Atmos.*
1185 *Sci*., 65: 2757–2783

1186 Phillips, V. T. J., C. Andronache, B. Christner, C. E. Morris, D. C. Sands, A. Bansemer, A.
1187 Lauer, C. McNaughton, and C. Seman, 2009: Potential impacts from biological aerosols
1188 on ensembles of continental clouds simulated numerically. *Biogeosciences*, 6, 987–1014,
1189 https://doi.org/10.5194/bg-6-987-2009.

1190 Phillips, V.T., P. J. Demott, C. Andronache, K.A. Pratt, K.A. Prather, R. Subramanian, and C.
1191 Twohy, 2013: Improvements to an Empirical Parameterization of Heterogeneous Ice
1192 Nucleation and Its Comparison with Observations. *J. Atmos. Sci*., 70, 378–
1193 409, https://doi.org/10.1175/JAS-D-12-080.1

1194 Pöhlker, C., D. Walter, H. Paulsen, T. Könemann, E. Rodríguez-Caballero, D. Moran-Zuloaga,
1195 J. Brito, S. Carbone, C. Degrendele, V. R. Després, F. Ditas, B. A. Holanda, J. W. Kaiser,
1196 G. Lammel, J. V. Lavrič, J. Ming, D. Pickersgill, M. L. Pöhlker, M. Praß, N. Löbs, J.
1197 Saturno, M. Sörgel, Q. Wang, B. Weber, S. Wolff, P. Artaxo, U. Pöschl, and M. O.
1198 Andreae, 2019: Land cover and its transformation in the backward trajectory footprint
1199 region of the Amazon Tall Tower Observatory, *Atmos. Chem. Phys*., 19, 8425–8470,
1200 https://doi.org/10.5194/acp-19-8425-2019.

1201 Pöhlker, M. L., C. Pöhlker, F. Ditas, F. and co-authors, 2016: Long-term observations of cloud
1202 condensation nuclei in the Amazon rain forest – Part 1: Aerosol size distribution,
1203 hygroscopicity, and new model parametrizations for CCN prediction, *Atmos. Chem.*
1204 *Phys*., 16, 15709–15740, https://doi.org/10.5194/acp-16-15709-2016.

1205 Pöhlker, M. L., F. Ditas, J. Saturno, T. Klimach, and co-authors, 2018: Long-term observations
1206 of cloud condensation nuclei over the Amazon rain forest – Part 2: Variability and

characteristics of biomass burning, long-range transport, and pristine rain forest aerosols, *Atmos. Chem. Phys*., 18, 10289–10331

Pöschl, U., S. T. Martin, B. Sinha, Q. Chen, S. S. Gunthe, J. A. Huffman, S. Borrmann, D. K. Farmer, R. M. Garland, G. Helas, J. L. Jimeney, S. M. King, A. Manzi, E. Mikhailov, T. Pauliquevis, M. D. Petters, , A. J. Prenni, P. Roldin, D. Rose, J. Schneider, H. Su, S. R. Zorn, P., Artaxo, and M. O. Andreae, 2010: Rainforest Aerosols as Biogenic Nuclei of Clouds and Precipitation in the Amazon. *Science*, 329, 1513–1516, doi:10.1126/science.1191056.

Pouzet, G., Peghaire, E., Aguès, M., Baray, J.-L., Conen, F., and Amato, P. (2017). Atmospheric Processing and Variability of Biological Ice Nucleating Particles in Precipitation at Opme, France. *Atmosphere,* 8(11):229.

Prenni, A. J., Y. Tobo, E. Garcia, P. J. DeMott, J. A. Huffman, C. S. McCluskey, S. M. Kreidenweis, J. E. Prenni, C. Pöhlker, and U. Pöschl, 2013: The impact of rain on ice nuclei populations at a forested site. *Geophy. Res. Lett*., 40, 227–231, doi:10.1029/2012GL053953.

Prenni, A. J., M. D. Petters, S. M. Kreidenweis, C. L. Heald, S. T. Martin, P. Artaxo, R. M. Garland, A. G. Wollny, and U. Pöschl, 2009: Relative roles of biogenic emissions and Saharan dust as ice nuclei in the Amazon basin. *Nat. Geosci.*, 2, 402– 405, doi:10.1038/ngeo517.

Priyamvada, H., R.K. Singh, M. Akila, R. Ravikrishna, R. S. Verma, S.S. Gunthe, 2017: Seasonal variation of the dominant allergenic fungal aerosols – One year study from southern Indian region. *Sci Rep* **7,** 11171 (2017).

Pruppacher, H. R., & J. D. Klett, 1997: Microphysics of clouds and precipitation. Dordrecht: Kluwer Academic Publishers.

1231 Pummer, B. G., H. Bauer, J. Bernardi, S. Bleicher, and H. Grothe, 2012: Suspendable
1232 macromolecules are responsible for ice nucleation activity of birch and conifer pollen,
1233 *Atmos. Chem. Phys*., 12, 2541–2550.

1234 Pummer, B. G., C. Budke, S. Augustin-Bauditz, D. Niedermeier, L. Felgitsch, C. J. Kampf, R.
1235 G. Huber, K. R. Liedl, T. Loerting, T. Moschen, M. SchauperlTollinger, C. E. Morris, H.
1236 Wex, H. Grothe, U. Pöschl, T. Koop, J. Fröhlich-Nowoisky, 2015: Ice nucleation by
1237 water-soluble macromolecules. *Atmos. Chem. Phys. 15* (8), 4077– 4091.

1238 Richard, C., J. G. Martin, and S. Pouleur, 1996: Ice nucleation activity identified in some
1239 phytopathogenic Fusarium species. *Phytoprotection*, 77, 83-92.

1240 Rogers R. R. and M. K. Yau, 1996: A short course in cloud physics,3rd ed., Butterworth-
1241 Heinemann, Woburn, Mass.

1242 Schnell R. C., S. N. Tan-Schnell, 1982: Kenyan tea litter: A source of ice nuclei. *Tellus*, 34,
1243 92-95.

1244 Schnell, R.C. and G. Vali, 1976: Biogenic Ice Nuclei: Part I. Terrestrial and Marine Sources. *J.*
1245 *Atmos. Sci.,* **33**, 1554–1564.

1246 Schrod, J., A. Danielczok, D. Weber, M. Ebert, E. S. Thomson, and H. G. Bingemer, 2016: Re-
1247 evaluating the Frankfurt isothermal static diffusion chamber for ice nucleation. *Atmos.*
1248 *Meas. Tech*., 9, 1313-1324, https://doi.org/10.5194/amt-9-1313-2016.

1249 Sesartic, A., U. Lohmann, and T. Storelvmo, 2012: Bacteria in the ECHAM5-HAM global
1250 climate model. *Atmos. Chem. Phys.*, 12, 8645–8661, https://doi.org/10.5194/acp-12-
1251 8645-2012.

1252 Shi, Z., L. Shao, T. P. Jones, A. G. Whittaker, S. Lu, K.A. Berube, T. He, R. J. Richards, 2003:
1253 Characterization of airborne individual particles collected in an urban area, a satellite city
1254 and a clean air area in Beijing, *Atmos. Environ*. 37, 4097–4108.

1255 Soo J. C., K. Monaghan, T. Lee, M. Kashon, and M. Harper, 2016: Air sampling filtration
1256 media: Collection efficiency for respirable size-selective sampling. *Aerosol Sci Technol*.
1257 2016 January; 50(1): 76–87.

1258 Stopelli, E., F. Conen, L. Zimmermann, C. Alewell, and C. E. Morris, 2014: Freezing
1259 nucleation apparatus puts new slant on study of biological ice nucleators in precipitation.
1260 *Atmos. Meas. Tech*., 7, 129-134.

1261 Tamer Vestlund, A., R. Al-Ashaab, S. F. Tyrrel, P. J. Longhurst, S. J. T. Pollard, G. H. Drew,
1262 2014: Morphological classification of bioaerosols from composting using scanning
1263 electron microscopy. *Waste Manag*. 34, 1101–1108.

1264 Vali, G., 1994: Freezing rate due to heterogeneous nucleation, *J. Atmos. Sci.*, 51
1265 (13), 1843– 1856.

1266 Vali, G., P. J. DeMott, O. Möhler, and T. F. Whale, 2015: Technical Note: A proposal for ice
1267 nucleation terminology. *Atmos. Chem. Phys*., 15, 10263–10270,
1268 https://doi.org/10.5194/acp-15-10263-2015.

1269 Vali, G., 1971: Quantitative Evaluation of Experimental Results an the Heterogeneous
1270 Freezing Nucleation of Supercooled Liquids. *J. Atmos. Sci.*, **28**, 402–409.

1271 Valsan, A.E., H. Priyamvada, R. Ravikrishna, V.R. Després, C.V. Biju, L.K. Sahu, A. Kumar,
1272 A., R.S.Verma, L. Philip, S.S. Gunthe, 2015: Morphological characteristics of
1273 bioaerosols from contrasting locations in southern tropical India – a case study. *Atmos.*
1274 *Environ*. 122, 321–331.

Valsan, A.E., R. Ravikrishna, C.V. Biju, C. Pöhlker, V.R. Després, J.A. Huffman, U. Pöschl, S.S. Gunthe, 2016: Fluorescent biological aerosol particle measurements at a tropical high-altitude site in southern India during the southwest monsoon season. *Atmos. Chem. Phys*. 16, 9805–9830

Whitehead, J. D., E. Darbyshire, J. Brito, H. M. J. Barbosa, I. Crawford, R. Stern, M. W. Gallagher, P. H. Kaye, J. D. Allan, H. Coe, P. Artaxo, and G. McFiggans, 2016: Biogenic cloud nuclei in the central Amazon during the transition from wet to dry season. *Atmos. Chem*., Phys., 16, 9727–9743, https://doi.org/10.5194/acp-16-9727-2016.

Wilson, T., L. Ladino, P. Alpert, *et al.*, 2015: A marine biogenic source of atmospheric ice-nucleating particles. *Nature*, 525**,** 234–238, https://doi.org/10.1038/nature14986.

Wittmaack, K. 2005: Brochosomes produced by leafhoppers-a widely unknown, yet highly abundant species of bioaerosols in ambient air. *Atmos. Environ*., 39, 1173-1180.

Wu, L., X. Li, H. Kim, H. Geng, R.H.M. Godoi, C.G.G. Barbosa, C.G.G., A.F.L. Godoi, C. I. Yamamoto, R.A.F. de Souza, C. Pöhlker, M.O.Andreae, C. U. Ro, 2019: Single-particle characteri-zation of aerosols collected at a remote site in the Amazonian rainforest and anurban site in Manaus, Brazil, *Atmos. Chem. Phys*. 19, 1221–1240.

Xia, Y., F. Conen, and C. Alewell, 2013: Total bacterial number concentration in free tropospheric air above the Alps. *Aerobiologia*, 29, 153–159.

Xu, F., L.P.R. de Craene, 2013: Pollen morphology and ultrastructure of selected species from Annonaceae. *Plant Syst Evol.,* 299, 11–24.

Tables:

Sr. No.	Type of aerosol sampling	Time (UTC)	Flow rate (sample volume)	Purpose	Instrument used in the analysis
1	0.2 µm filter only	1400-1450	4 Lpm (200 L)	Immersion freezing IN	FRIDGE-IMM
2	PEAC7	1500-1550	2 Lpm (100 L)	Deposition and condensation-freezing IN, SEM	FRIDGE-STD, SEM
3	Cascading Filtering, Day	1600-2010	4 Lpm (1000 L)	SEM, Biological IN	LINDA, SEM, flow cytometry
4	Cascading Filtering Overnight	2030-1230 (next day)	1.5 Lpm (1440 L)	SEM, Biological IN	LINDA, SEM, flow cytometry

Tabe 1: Daily sampling plan along with sampling type, time duration, flow rate, volume sampled, sampling purpose, and the instrument used for sample analysis.

Sample	Sample Vol. in L Filters (Si wafers)	Scanned Area in % Filters (Si wafers)	Total images Filters (Si wafers)
0911N	1500 (100)	0.14 (0.064)	302 (101)
0912D	1000 (100)	0.1 (0.062)	201 (114)
0913D	100 (100)	0.11 (0.07)	210 (103)

Table 2: Details of SEM analysis including samples volume, scanned area of filter and Si wafer, the number of bioaerosol images collected.

PBAP type	Typical size (μm) and number conc. (m^{-3} of air)	General morphological features	References
Fungal spores	Size: 1-50; most frequently 2-10 Concentration: 10^4	(i) shape: globose, elliptical, fusiform, asymmetric, lemon-shaped, barrel-shaped, curved (ii) wall characteristics: smooth, granular, reticulate, spines, warts (iii) attachment scars, attachment pegs (iv) other features: branched hyphae	Després et al. (2012) and references therein, Priyamvada et al. 2017, Li et al. 2020, Huffman et al. 2012, Cybelli et al. 2018, China et al. 2016,
Bacteria	Size: 0.5-4 Concentration: 10^4 (over land), 10-1000 (over ocean)	(i) shape: spherical, rodlike, helical (ii) wall: flagella, pili, capsules (iii) Arrangement: pairs, tetrads, clusters, chains	Després et al. (2012) and references therein, Li et al. 2020
Pollen	Size: 10-50 Concentration: 10-1000	(i) shape: ellipsoid, fusiform, globose/spheroidal (ii) presence of forrows (iii) outer exine is usually sculptured (iv) exine ornamentation like fossulate or microrugulate	Després et al. (2012) and references therein, Cybelli et al. 2018 and references therein, Xu et al. 2013
Plant/animal detritus	Size: brochosomes-0.5, leaf litter 0.5-5 Concentration: NA	Various shapes (i) shape: football (brochosomes), spiral (epicuticular wax of plants), elongated (leaf litter)	Després et al. (2012) and references therein, Wittmaack, 2005
Algae	Size: 1-10 Concentration: 100	(i) shape: Unicellular flagellates or amoeboids, colonial and nonmotile forms	Després et al. (2012) and references therein

Table 3: Typical size ranges, concentrations in air and general morphological characteristics of different PBAPs, based on literature available. Based on this information, PBAPs have been classified into different groups. Also enlisted are various studies referred to for classification of PBAPs.

PBAP group	Typical Size	Mean number concentration (m^{-3} air) from SEM analysis
Fungal spores and associated fragments	1-10 µm	7.6×10^4 $(\mp 2.8 \times 10^4)$
Bacteria and their fragments	0.5-2 µm	4.2×10^5 $(\mp 1.98 \times 10^5)$
Pollen and their fragments	6-50 µm	1.07×10^3 (∓ 673)
Viral, plant/animal detritus	0.2-5 µm	4.1×10^5 $(\mp 1.8 \times 10^5)$

Table 4: General size and mean number concentration of various PBAP groups based on our SEM analysis.

Symbol	Value
$\gamma_{fng}, \gamma_{pln}, \gamma_{bct}, \gamma_{dts}$	$0.5\ \mathrm{C}^{-1}$
$\omega_{FNG,1*}$	$2.1 \times 10^{-4}\ \mathrm{m}^2$
$\omega_{PLN,1*}$	$0.1\ \mathrm{m}^2$
$\omega_{BCT,1*}$	$2.51 \times 10^{-4}\ \mathrm{m}^2$
$\omega_{DTS,1*}$	$0.1\ \mathrm{m}^2$
$T_{FNG,1}, T_{fng,2}$	$-7\ ^{o}\mathrm{C}, -2\ ^{o}\mathrm{C}$
$T_{PLN,1}, T_{pln,2}$	$-10\ ^{o}\mathrm{C}, -7\ ^{o}\mathrm{C}$
$T_{BCT,1}, T_{bct,2}$	$-7\ ^{o}\mathrm{C}, -2\ ^{o}\mathrm{C}$
$T_{DTS,1}, T_{dts,2}$	$-10\ ^{o}\mathrm{C}, -7\ ^{o}\mathrm{C}$

Table 5: Details about most empirical parameters mentioned in section 4.1 and 4.2 together with their values.

1366

Species	Reference	Obs. Mass (kg m^{-3}) or Number conc. (m^{-3})	IN conc. (m^{-3}) (in bracket temp in ºC)
Fungi	1. O'Sullivan et al. (2015): Nucleation sites g^{-1} at –5, –10, and –15ºC are 2.5×10^5, $4.\times 10^7$, $2.\times 10^8$ respectively	*Mass:* 1.51×10^{-9} (0911N) 1.52×10^{-9} (0912D) 1.17×10^{-9} (0913D)	For 0911N: 0.38 (-5), 60.63 (-10), 303.16 (-15) For 0912D: 0.37 (-5), 60.5 (-10), 302.53 (-15) For 0913D: 0.29 (-5), 46.8 (-10), 234.4 (-15)
	2. Haga et al. (2014): Active IN per fungi at -10 and –15ºC are $5.\times 10^{-4}$, $7.\times 10^{-4}$ respectively.	*Conc.* 1.01×10^5 (0911N) 0.73×10^5 (0912D) 0.49×10^5 (0913D)	For 0911N: 52.80 (-10), 73.93 (-15) For 0912N: 36.9 (-10), 51.70 (-15) For 0913N: 24.81 (-10), 34.74 (-15)
Pollen	1. O'Sullivan et al. (2015) (used in construction of scheme): Nucleation sites g^{-1} at –10, –15ºC are 2×10^3, $10.\times 10^3$respectively.	*Mass:* 5.76×10^{-10} (0911N) 5.14×10^{-10} (0912D) 1.18×10^{-10} (0913D)	For 0911N: 1.15×10^{-3} (-10), 5.76×10^{-3} (-15) For 0912D: 1.02×10^{-3} (-10), 5.14×10^{-3} (-15) For 0913D: 2.36×10^{-4} (-10), 1.18×10^{-3} (-15).
	2. Murray et al. (2012)		Pollen as Potential IN is $2.\times 10^{-3}$ (-15)
Bacteria	1. Joly et al. (2014): Bacterial conc. was variable from 1.6×10^3 to 3.4×10^4 mL^{-1} Mean fraction of ice nucleation active bacteria at -6, -8, and -12 ºC are 0.01, 0.18, and 1.02% respectively. Liquid water content was assumed 0.5 g/m^3.		0.32 (-6), 5.8 (-8), 32.5 (-10)
Leaf Litter	1. Schnell and Tan-Schnell (1982): Nucleus concentration (g^{-1}) at –6.5ºC and –10ºC is 60 and 800 respectively (used in construction of scheme).	*Mass:* 3.86×10^{-10} (0911N) 2.56×10^{-11} (0912D)	For 0911N: 2.3×10^{-5} (-6.5), 3.08×10^{-4} (-10)

		2.67×10^{-10} (0913D)	For 0912D: 1.5×10^{-6} (-6.5), $2.\times 10^{-5}$ (-10) For 0913D: 1.6×10^{-5} (-6.5), 2.13×10^{-4} (-10)
	2. Schnell and Vali (1976): Nucleus concentration (g^{-1}) at –7°C and -12 7°C is 100 and at is 1000 respectively. (for leaf litter in tropical climate zone)		For 0911N: 3.8×10^{-5} (-7), 3.8×10^{-4} (-12), For 0912D: 2.5×10^{-5} (-7). 2.5×10^{-4} (-12). For 0913D: 2.67×10^{-5} (-7), 2.67×10^{-4} (-12),
Total biological IN	Pouzet et al. 2017 (Figure 1). Rainwater content was assumed 0.3 gm/m^3 to convert concentrations to per m^3 of the air.		0.06 (-5), 1.65 (-10), 6 (-12)

Table 6: Origin of estimations of various biological IN concentrations shown in figure 7. The mass of bioaerosol particles was calculated assuming aerosol particles to be spherical with a density of 1000 kg m^{-3}. Observation of IN activity of pollen and leaf litter used in the construction of the scheme are mentioned in brackets.

1379

Notation	Description	Value and Units
D	Diameter	m
f_{algae}	Frozen fraction of algal particles from Wilson et al. (2015).	
H_X	Fraction reducing ice nuclei activity at low S_i, warm T	
MAX	Maximum value	
MIN	Minimum value	
$n_{IN\_BIO,X}$	Contribution to total biological IN from group X	kg^{-1}
$n_{s,}$	Ice-active surface site density	m^{-2}
n_m	Ice-active mass site density	kg^{-1}
n_X	Number mixing ratio of particles in PBAP group X	kg^{-1}
n_{IN_BIO}	Total number m.r. of active biological IN predicted	kg^{-1}
$n_{IN\_BIO,X}$	Contribution to n_{IN_BIO} from PBAP group X	kg^{-1}
$n_{X,a}$	Number of aerosols in PBAP group X	kg^{-1}
$n_{X,cn}$	Number mixing ratio of contact IN for group X	kg^{-1}
$n_{X,a,liq}$	Number of interstitial IN in group X lost by becoming immersed	kg^{-1}
$n_{X,\mathrm{imm}}$	Number of IN from group X immersed in cloud liquid	kg^{-1}
Q_r	Mixing ratio of rain	kg kg^{-1}
Q_X	Mixing ratio of aerosol in group X	kg kg^{-1}
RH_{ice}	Relative humidity over ice	%
S_i	Saturation ratio of vapor with respect to ice	
t	Time	s
T	Temperature	^oC
$T_{X,1}$	Colder threshold temperature for onset of freezing for group X	^oC
$T_{X,2}$	Warmer threshold temperature for onset of freezing for group X	^oC
v_t	Fall speed of raindrop in given size bin	m s^{-1}
w	Vertical velocity of air	m s^{-1}
X	Label for four PBAP groups (Fungal spores and associated fragments (FNG), Pollen and their fragments (PLN), Bacteria and their fragments (BCT), Viral, Plant/animal detritus (DTS), and Algae (ALG))	
$\xi(T)$	Fraction that is zero for $T > T_{X,2}$ (^{o}C) and 1 for $T < T_{X,1}$ (^{o}C), being $\delta_1^0(T, T_{X,1}, T_{X,2})$ for $T_{X,1} < T < T_{X,2}$ (^{o}C) for X= FNG, PLN, BCT, DTS	$0 \leq \xi \leq 1$
Ω_X	Total surface area of all bioaerosols > 0.1 µm in diameter in group X.	[aerosol] m^2 [air] kg^{-1}
$\Omega_{X,int}$	Interstitial component of Ω_X	[aerosol] m^2 [air] kg^{-1}
$\Omega_{X,rain}$	Total surface area of all aerosols with D > 0.1 µm in group X inside raindrops	[aerosol] m^2 [air] kg^{-1}

$\delta_a^b\,(y, y_1, y_2)$	Cubic interpolation function equal to a at y ≤ y_1 and to b for ≥ y ≤ y_2 While $\delta_a^b = a_0 + a_1 y + a_2 y^2 + a_3 y^3$ for $y_1 < y < y_2$, where $a_{0=} B, a_1 = A y_1 y_2, a_2 = -\frac{A(y_1+y_2)}{2}$, and $a_3 = \frac{A}{3}$ with $A = \frac{6(a-b)}{(y_2-y_1)^3}$ and $B =$ a $+ \frac{A y_1^3}{6} - \frac{A y_1^2 y_2}{2}$ (adopted from Phillips et al. 2008)	
μ_X	Average number of ice embryos per aerosol particle	
γ_X	Slope value of the fit for $X =$ FNG, PLN, BCT, and DTS each of four PBAP group.	$^oC^{-1}$.
α_X	Fraction of $n_{IN,1,*}$ from IN activity group X= {DM, BC, O, solO}	{2/3, 1/3-0.06, 0.06}
$\omega_{X,1*}$	Baseline coefficient of PBAP for *X*= FNG, PLN, BCT, and DTS	m^2
Δt	Model time step	s
ΔT_{CIN}	Diff. in freezing temperature between contact and bulk water modes.	4.5^{o}C

Table A1: Symbols used in this paper, along with their descriptions and units.

Figures:

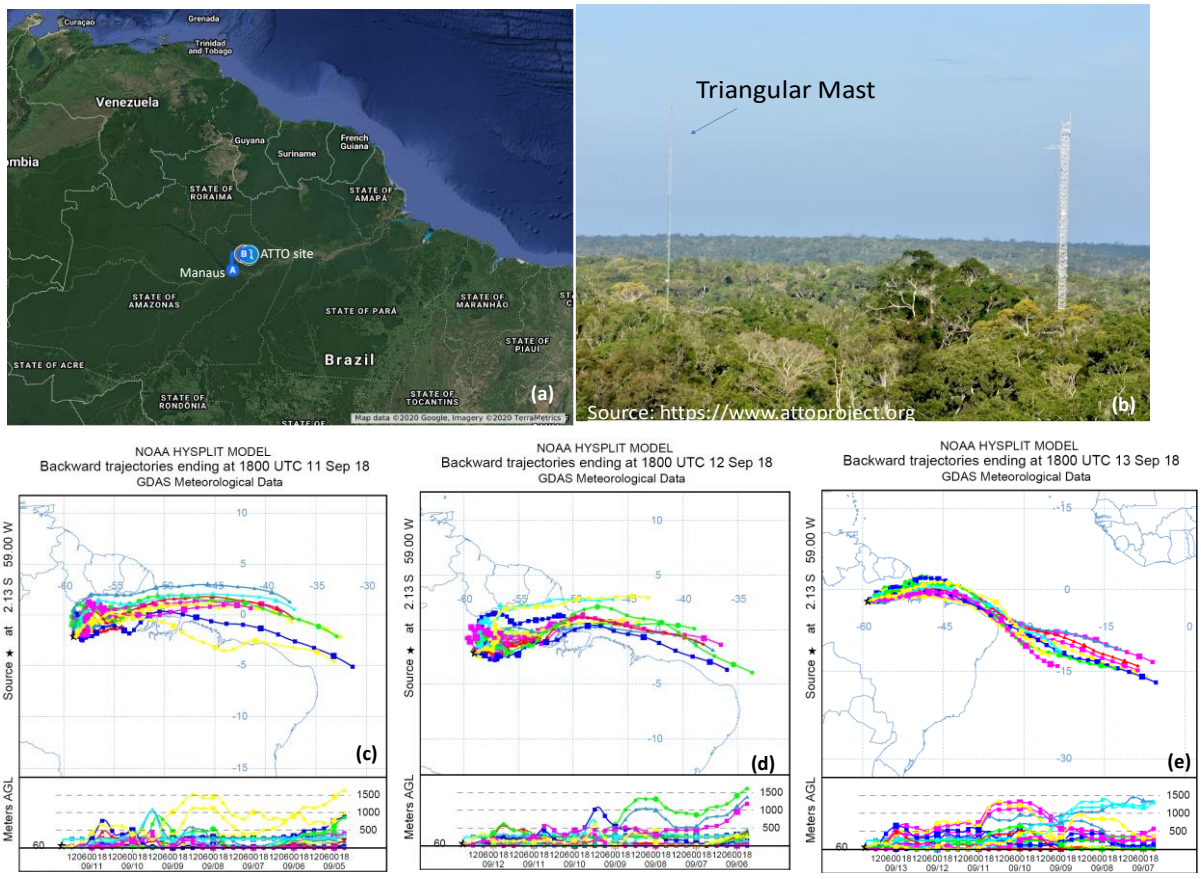

FIG. 1. Location of the ATTO site and Manaus in the central Amazon rainforest (source Google maps) (a). The sampling location at the ATTO site include a triangular mast on which a Total Suspended Particles (TSP) inlet was installed at 60 m above ground (b). The HYSPLIT seven-days (168 h) ensemble backward trajectories (c, d, and e) for three typical sampling days (Sept. 11-13, 2018) are shown for an endpoint altitude of 60 m.

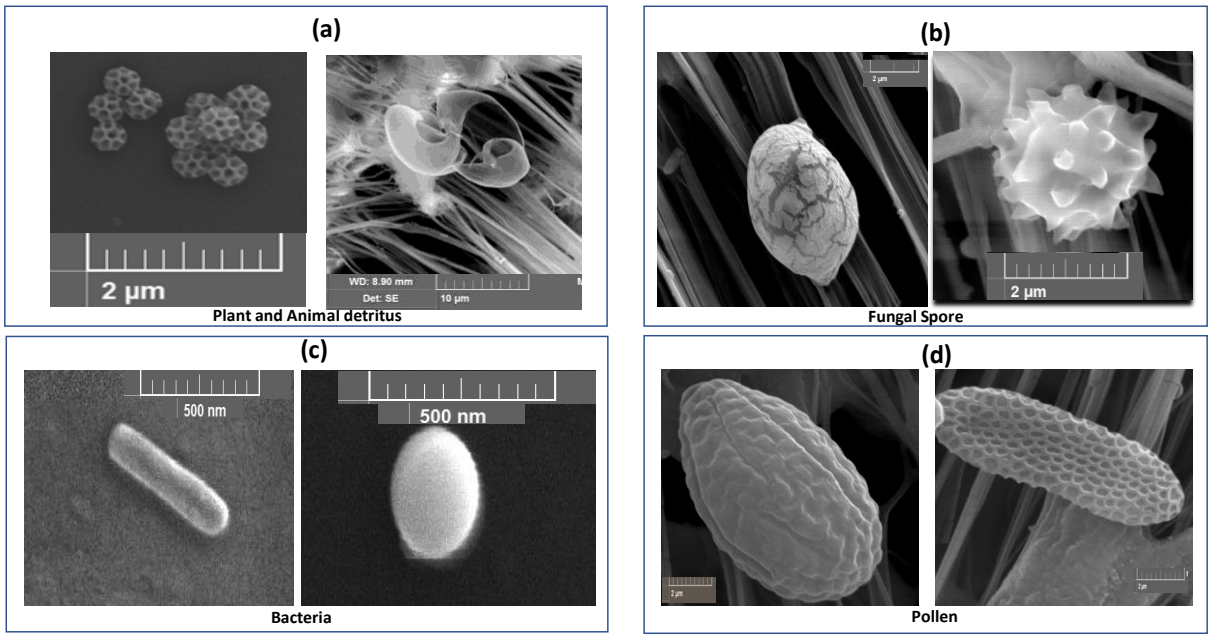

1403

1404 FIG. 2. Representative scanning electron microscopy images of brochosomes and leaf litter
1405 (group: plant and animal detritus) (a), fungal spore (b), bacteria (c) and pollen (d) from 0911N,
1406 0912D and 0913D. Scale is varying for each image and is shown separately.

1407

1408

1409

1410

1411

1412

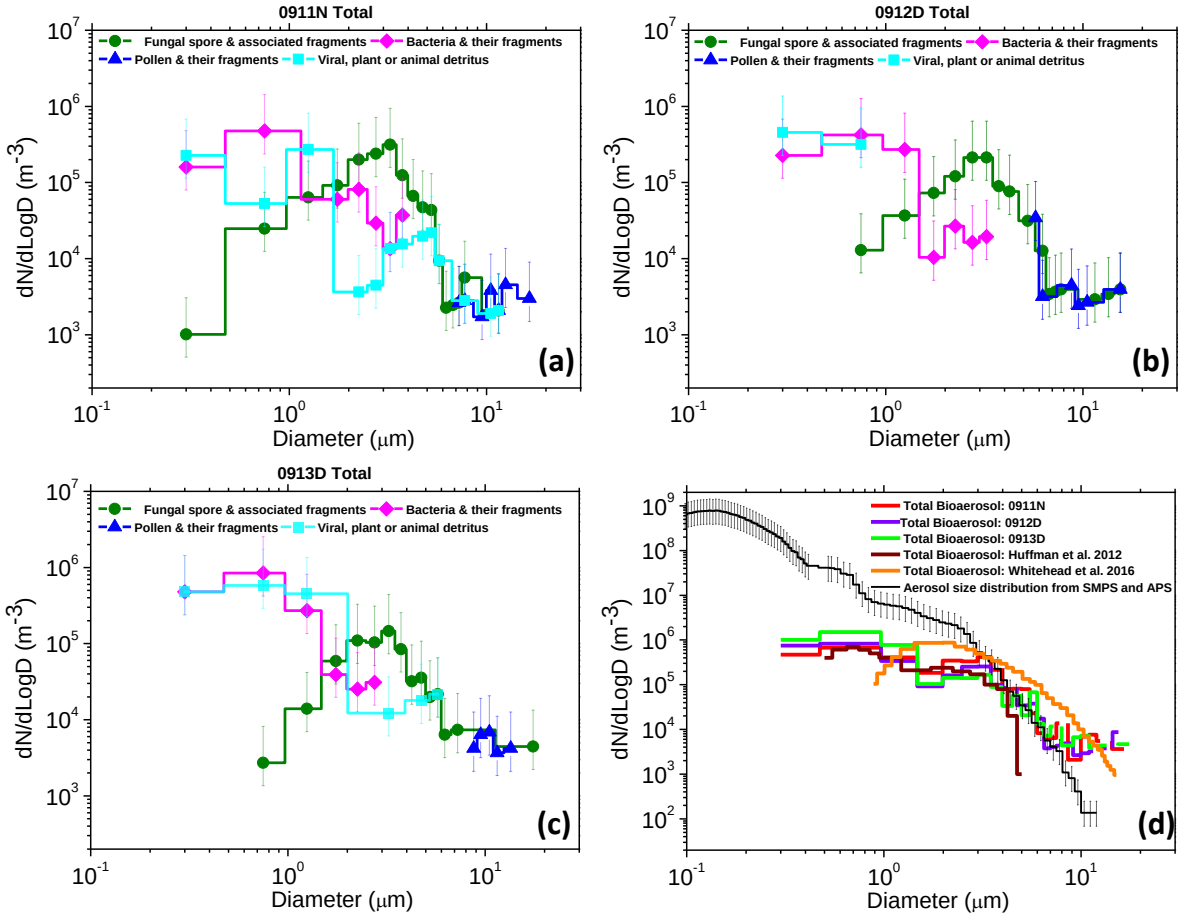

FIG. 3. The size distribution of PBAPs based on SEM analysis of samples 0911N, 0912D, and 0913D (a, b, and c). The size distribution of PBAPs shown here is from the combination of 5 and 1.2 μm filters. The total PBAP size distribution from each day is compared with the literature data (d). The total PBAP size distribution from our observations include unidentified PBAPs in addition to the other PBAP groups considered for classification.The combined aerosol size distribution from SMPS and APS on 0914 (thin black line) is also shown for reference.

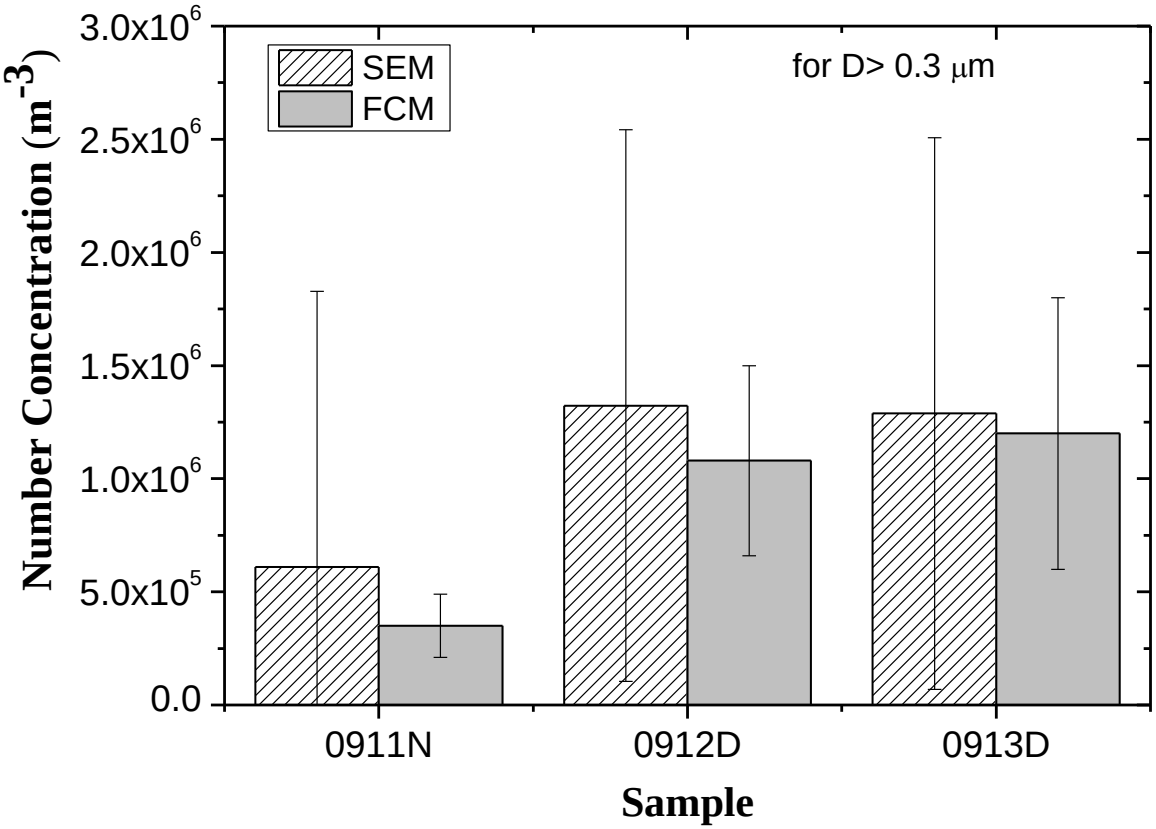

FIG. 4. Comparison of total bioaerosol particle number concentration (D > 0.3 μm) measured by Scanning Electron Microscopy (SEM; left bars) with Flow Cytometry (FCM; right bars). Error bars for number concentrations measured by FCM were estimated based on independent runs of FCM for the same sample.

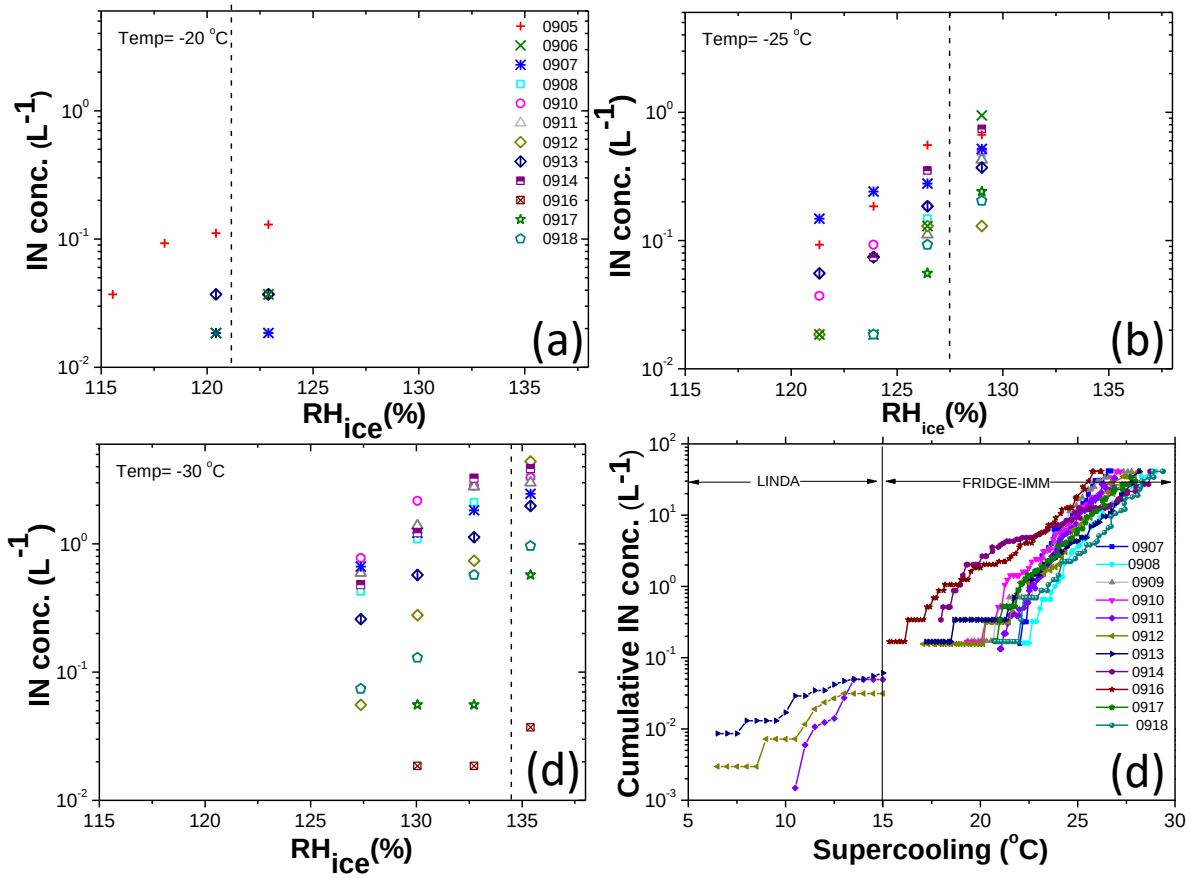

FIG. 5. The concentration of IN activated by deposition and condensation freezing mode in the FRIDGE-STD chamber at −20°C (a), −25°C (b), and −30°C (c). The dotted vertical lines in a, b, and c indicate saturation w.r.t. water. Cumulative IN concentrations activated by immersion freezing mode from separate experiments in FRIDGE-IMM are shown(d). The cumulative immersion freezing IN concentrations for 0911N, 0912D, 0913D from analysis in LINDA are also shown.

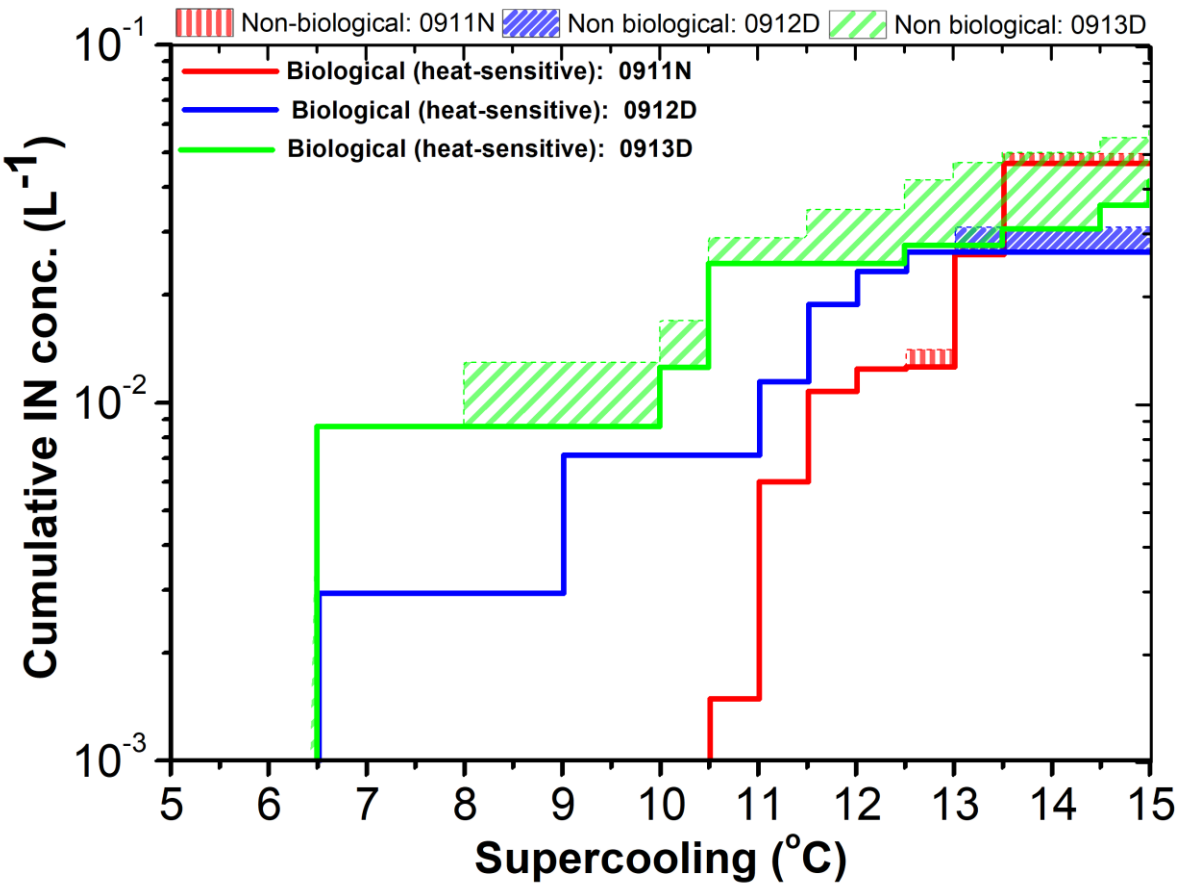

FIG. 6. Cumulative concentrations of biological (heat sensitive, bold lines) and non-biological (heat-resistance, shaded area) IN. The sum of two categories corresponds to the concentrations of total IN. The lower bound was considered for values below the detection limit. The IN concentrations shown here are from 5 and 1.2 µm filters processed in LINDA.

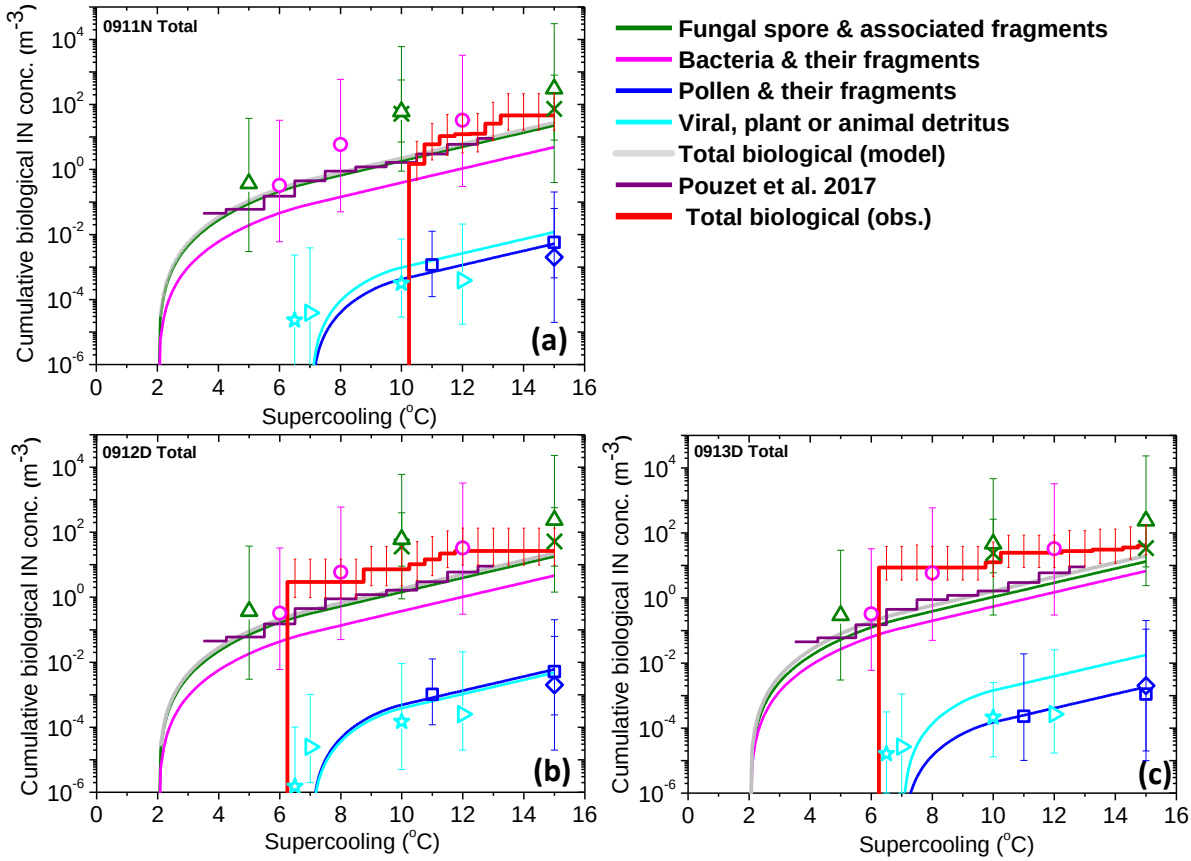

FIG. 7. Prediction of biological ice nuclei concentrations by new empirical parameterization based on size distribution of PBAPs, shown as a function of temperature for various bioaerosol species. The total biological ice nuclei concentrations from the empirical parametrization (thick black line) are compared with the observed values (thick red) from the drop freezing experiments with LINDA. The prediction is based on the total size distribution (5 +1.2 µm) for each sampling day shown here. In addition, predicted values of biological IN are compared to previous observations listed in Table 5. Biological ice nuclei concentration of fungi based on active fractions measured by Haga et al. (2014) (green crosses) and O'Sullivan et al. (2015) (green triangles) are shown for comparison. The number concentrations of pollen as biological ice nuclei are shown based Murray et al. (2012) (blue diamonds) and O'Sullivan et al. (2015) (blue squares). The bacterial ice nuclei concentrations based on Joly et al. 2014 (magenta circles). The leaf litter as ice nuclei are also shown based on Schnell Tan-Schnell (1982),

Schnell and Vali (1976). Black dotted lines in the plot of 1.2 μm filter represent the upper and lower bounds in predicting ice nuclei concentrations due to uncertainties in collection efficiency.

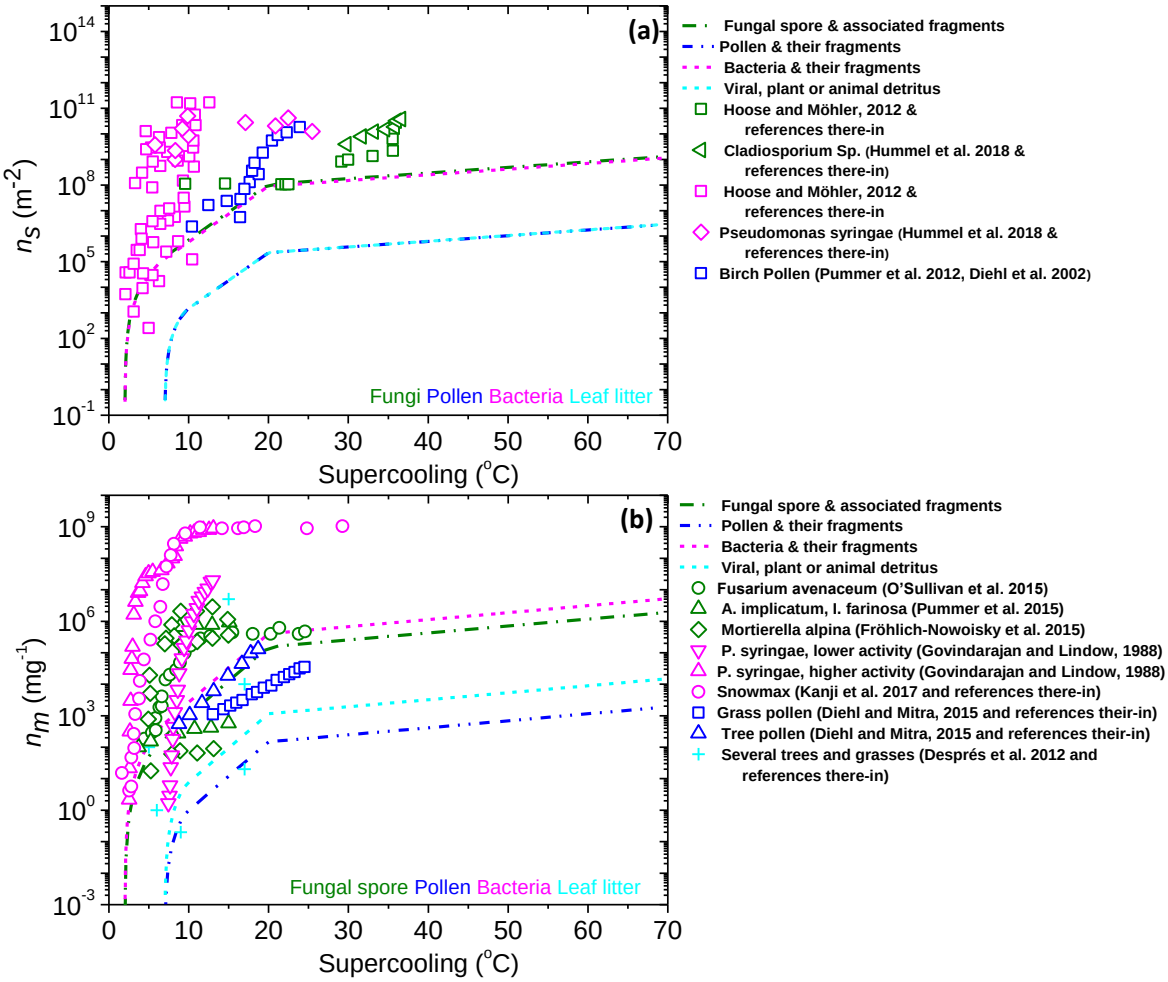

1492

1493 FIG. 8. Ice-active surface site densities (n_s) (a) and ice-active mass site density (b) for various
1494 PBAP groups from the proposed empirical parameterization (dotted lines) are shown as a
1495 function of temperature. The values for these two parameters from previous studies are also
1496 shown for a few biological species of PBAPs.

1497

1498

1499

1500

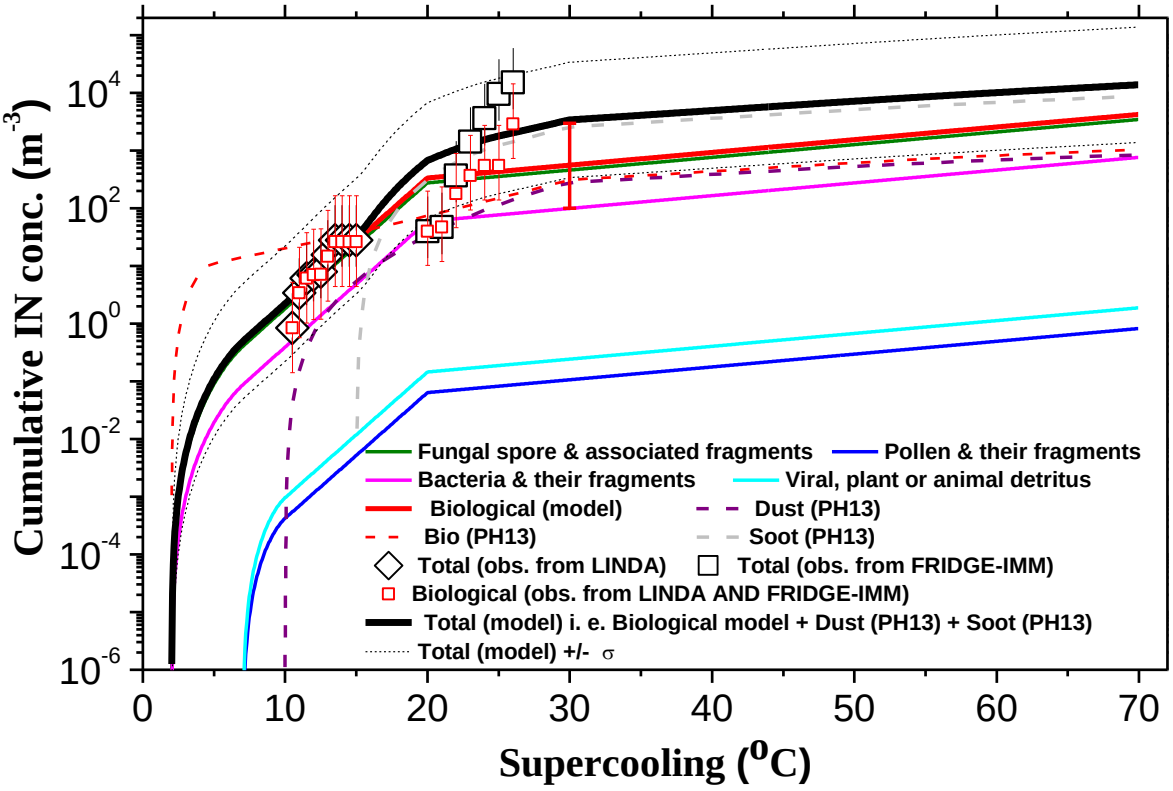

FIG. 9. The number concentration of biological ice nuclei predicted by empirical parameterization as a function of supercooling in a water-saturated air parcel. The number concentrations of dust, soot, and biological ice nuclei predicted by the empirical ice nucleation scheme by Phillips et al. (2013) (mentioned as PH13 in the plot) are also shown for comparison. The error bars of observed IN concentrations indicates the standard deviations estimated based on the uncertainties in the measurements. An error bar in bold red on the Biological (model) line indicated uncertainties in the estimated biological IN at temperature colder than −15°C.

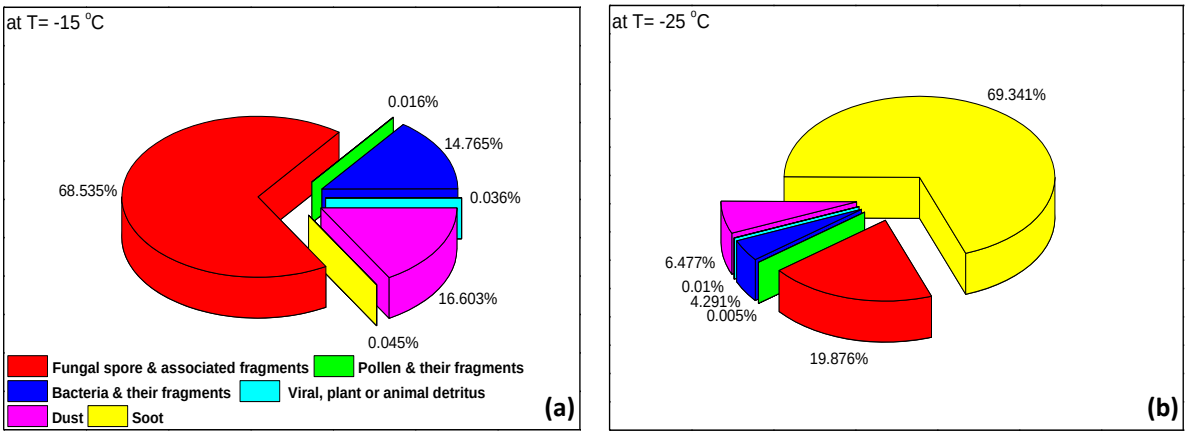

FIG. 10. The pie chart shows the relative contributions to the total IN concentration of the different PBAP groups as well as dust and soot particles at T= −15°C (a) and T= −25°C for the parcel model simulation shown in Figure 9.

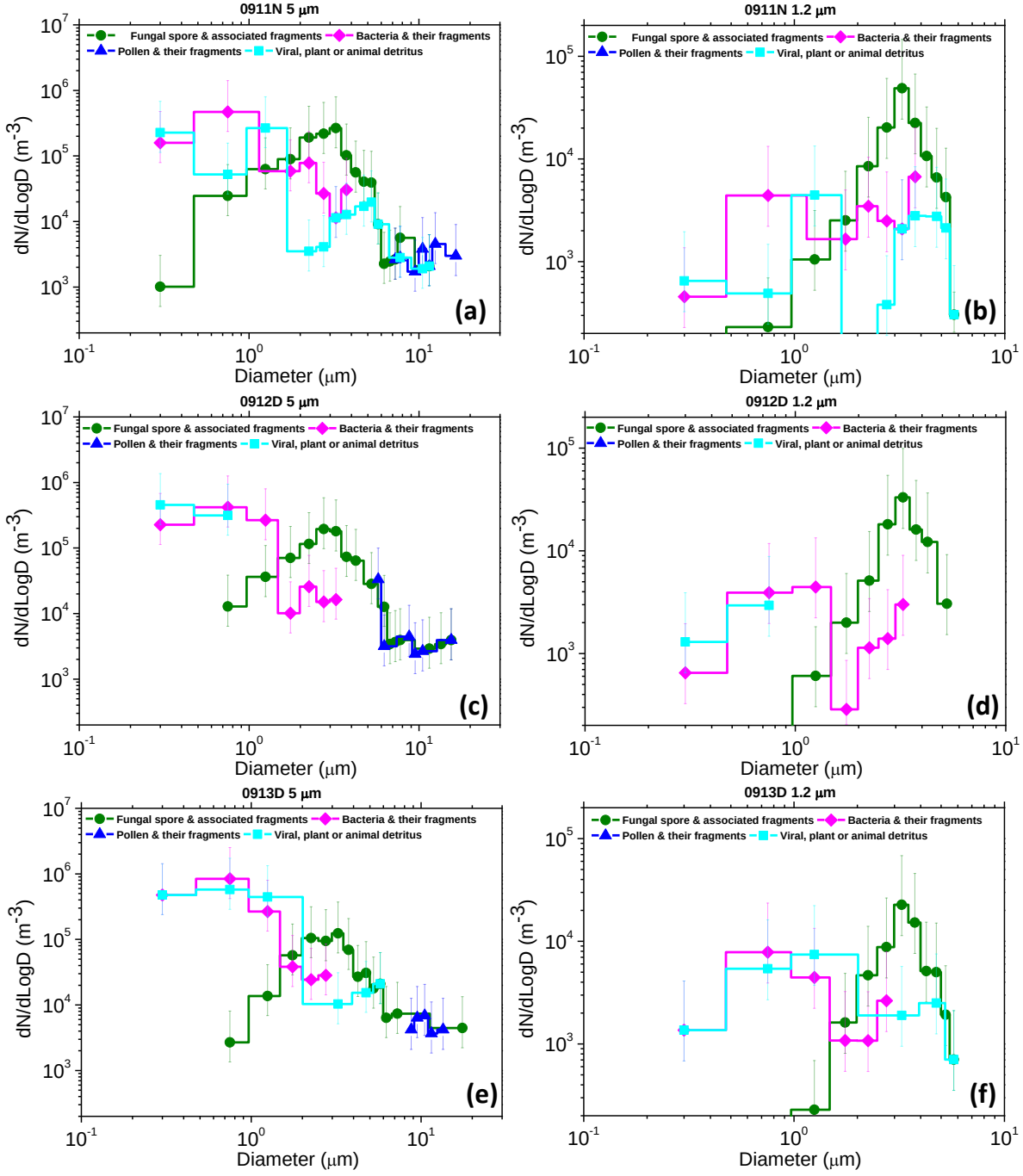

Figure B1: The size distribution of PBAPs based on SEM analysis of 5 µm and 1.2 µm filter.

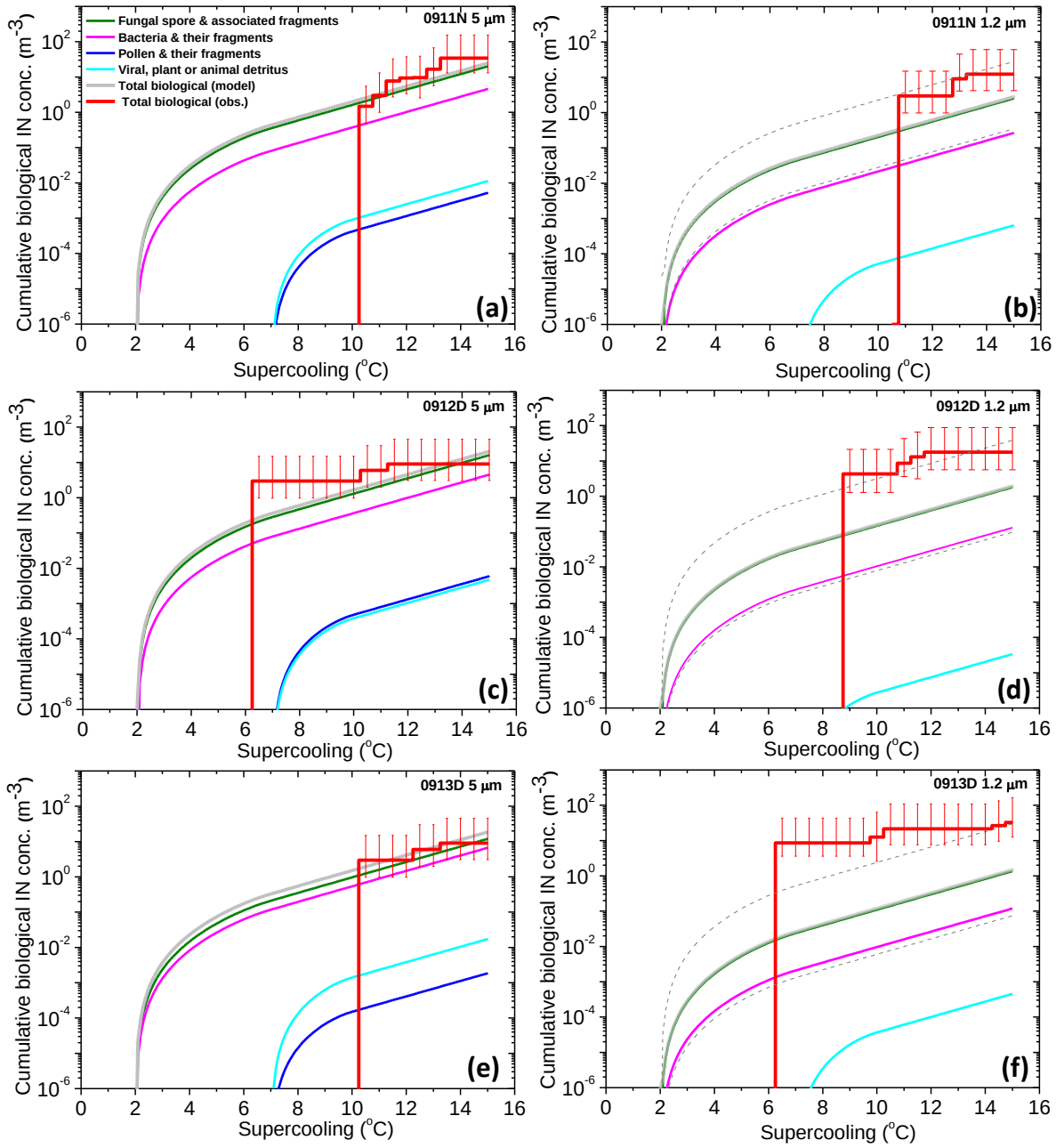

Figure C1: Prediction of biological ice nuclei concentrations by new empirical parameterization based on size distribution of PBAPs in 0911N, 0912D and 0913D shown as a function of temperature for various bioaerosol species. The total biological ice nuclei concentrations from the empirical parametrization (thick black line) are compared with the

observed values (thick red) from the drop freezing experiments with LINDA. For each case, the prediction is based on PBAP size distribution from 5 µm, and 1.2 µm and is shown separately. Black dotted lines in the plot of 1.2 µm filter represent the upper and lower bounds in predicting ice nuclei concentrations due to uncertainties in collection efficiency.